

## Neurobiology

## Inhibition of Autophagy Prevents Hippocampal Pyramidal Neuron Death after Hypoxic-Ischemic Injury

Masato Koike,\* Masahiro Shibata,\*  
Masao Tadakoshi,\* Kunihiro Gotoh,\*  
Masaaki Komatsu,<sup>†‡</sup> Satoshi Waguri,<sup>§</sup>  
Nobutaka Kawahara,<sup>¶</sup> Keisuke Kuida,<sup>||</sup>  
Shigekazu Nagata,\*\* Eiki Kominami,<sup>†</sup>  
Keiji Tanaka,<sup>‡</sup> and Yasuo Uchiyama\*

From the Department of Cell Biology and Neurosciences,\* Osaka University Graduate School of Medicine, Osaka, Japan; the Department of Biochemistry,<sup>†</sup> Juntendo University School of Medicine, Tokyo, Japan; the Department of Anatomy and Histology,<sup>‡</sup> Fukushima Medical University School of Medicine, Fukushima, Japan; the Department of Neurosurgery,<sup>§</sup> Graduate School of Medicine, University of Tokyo, Tokyo, Japan; the Department of Medical Chemistry,<sup>¶</sup> Graduate School of Medicine, Kyoto University, Kyoto, Japan; the Laboratory of Frontier Science,<sup>||</sup> Tokyo Metropolitan Institute of Medical Science, Tokyo, Japan; and Vertex Pharmaceuticals,<sup>§</sup> Cambridge, Massachusetts

Neonatal hypoxic/ischemic (H/I) brain injury causes neurological impairment, including cognitive and motor dysfunction as well as seizures. However, the molecular mechanisms regulating neuron death after H/I injury are poorly defined and remain controversial. Here we show that Atg7, a gene essential for autophagy induction, is a critical mediator of H/I-induced neuron death. Neonatal mice subjected to H/I injury show dramatically increased autophagosome formation and extensive hippocampal neuron death that is regulated by both caspase-3-dependent and -independent execution. Mice deficient in Atg7 show nearly complete protection from both H/I-induced caspase-3 activation and neuron death indicating that Atg7 is critically positioned upstream of multiple neuronal death executioner pathways. Adult H/I brain injury also produces a significant increase in autophagy, but unlike neonatal H/I, neuron death is almost exclusively caspase-3-independent. These data suggest that autophagy plays an essential role in triggering neuronal death execution after H/I injury and Atg7 represents an attractive therapeutic target for

minimizing the neurological deficits associated with H/I brain injury. (*Am J Pathol* 2008, 172:454–469; DOI: 10.2353/ajpath.2008.070876)

Neonatal hypoxic/ischemic (H/I) brain injury causes neurological impairment, including cognitive and motor dysfunction as well as seizures.<sup>1,2</sup> The patterns of neuron death after H/I injury in rodent models appear similar to those involved in human cases of H/I encephalopathy.<sup>3–6</sup> Morphological and biochemical approaches have shown the presence of apoptotic and necrotic neuron death in the pyramidal layer of the hippocampus after H/I injury,<sup>7</sup> whereas the extent of damage from H/I injury depends on the degree of brain maturation and the severity of the insult.<sup>8–10</sup> Apoptotic neuron death after H/I injury is accompanied by the activation of caspases, which may be associated with proapoptotic factors such as Bax<sup>11,12</sup> or Bad,<sup>13</sup> and suppressed by anti-apoptotic factors such as Bcl-xL.<sup>14</sup> Although many neuroprotective strategies have been proposed, few anti-apoptotic therapies have proven to be useful in inhibiting H/I-induced brain injury.<sup>15</sup> Therefore, it is very important to understand what molecular pathways are executed in neuron death induced by H/I brain injury.

Autophagy, which is a highly regulated process involving the bulk degradation of cytoplasmic macromolecules and organelles in mammalian cells via the lysosomal system, is induced under starvation, differentiation, and normal growth control to maintain cellular homeostasis and survival.<sup>16–18</sup> Simultaneously, it has also been evident that autophagy participates in various neurodegen-

Supported by the Japan Society for the Promotion of Science from the Ministry of Education, Science, Sports, and Culture, Japan (grant-in-aid for scientific research 16GS0315 to Y.U., M.S., and M.K.).

Accepted for publication October 23, 2007.

Supplemental material for this article can be found on <http://ajp.amjpathol.org>.

Address reprint requests to Yasuo Uchiyama, Department of Cell Biology and Neurosciences, Osaka University Graduate School of Medicine, 2-2 Yamadaoka, Suita, Osaka 565-0871, Japan. E-mail: y-uchi@anat1.med.osaka-u.ac.jp.

erative disorders<sup>19-22</sup> and further that it can trigger a form of cell death distinct from apoptosis in neurons.<sup>23-26</sup> In particular, we have previously shown that autophagy is highly induced in CA1 pyramidal neurons of gerbil hippocampus after brief forebrain ischemia, whereas such neurons that contain numerous autophagosomes/autolysosomes in the perikarya undergo delayed neuronal death.<sup>27</sup> The induction of autophagy has been shown in neonatal and adult mouse cortex and striatum after H/I injury,<sup>10,28</sup> and LC3, a marker protein for autophagy, is required for autophagosome formation via its conversion from LC3-I to LC3-II.<sup>29</sup> However, it is unclear if autophagy participates as a pro- or anti-death factor in the execution of neuron death after H/I injury.<sup>30</sup>

Here, to elucidate the molecular mechanisms of pyramidal neuron death in the hippocampus after H/I injury, we used an ischemia model of left carotid artery occlusion followed by exposure to low oxygen<sup>31</sup> and found that H/I injury-induced pyramidal neuron death in the neonatal hippocampus occurred using both caspase-dependent and -independent pathways. In such damaged neurons autophagy was strongly induced, and this ischemic neuronal death was rescued by an Atg7 deficiency. These data indicate that autophagy plays an essential role in the execution of pyramidal neuron death in the neonatal mouse hippocampus after H/I injury.

## Materials and Methods

### Animals

The experiments described below were performed in compliance with the regulations of Osaka University Graduate School of Medicine's Guidelines for the Care and Use of Laboratory Animals. Neonatal and adult C57BL/6J mice at postnatal day 7 (P7) and 8 weeks of age were obtained from CLEA Japan (Tokyo, Japan) or Charles River Laboratories Japan (Yokohama, Japan). Nestin-Cre transgenic mice [strain name: B6.Cg(SJL)-Tg(nestin-Cre)1Kln/J]<sup>32</sup> were purchased from the Jackson Laboratory (Bar Harbor, ME). *Atg7<sup>fllox/fllox</sup>* mice,<sup>16</sup> *CAD* homozygous (-/-) mice,<sup>33</sup> and *caspase-3* heterozygous (+/-) mice backcrossed onto a C57BL/6 background for at least 10 generations<sup>34,35</sup> were transferred to the Institute of Experimental Animal Sciences, Osaka University Graduate School of Medicine, and were housed in a pathogen-free facility. *Atg7<sup>fllox/fllox</sup>* mice were bred with nestin-Cre transgenic mice to produce *Atg7<sup>fllox/fllox</sup>*; nestin-Cre mice.<sup>36</sup> *Caspase-3<sup>+/-</sup>* mice were crossed to obtain a mixture of +/+, +/-, and -/- pups. To determine the genotypes of these lines, genomic DNA was prepared from pup tail snips and analyzed by polymerase chain reaction (PCR). The following primer sets were used for genotyping: for the Cre transgene, 5'-TTTGCTGCAT-TACCGGTGATGCAAC-3' and 5'-TGCCCTGTTTACATATCCAGGTTACGGA-3'; wild-type and *Atg7<sup>fllox</sup>* alleles, 5'-TGGCTGCTACTTCTGCAATGATGT-3' and 5'-CAGGACAGACCATCAGCTCCAC-3';<sup>16</sup> wild-type and mutant *CAD* alleles, 5'-AAAAGAACAGTCGGGACTGC-3', 5'-GATTGCCAGCGCATCGCCTT-3', and 5'-TTCACACCAG-

GAGACATCTG-3';<sup>33</sup> wild-type and mutant *caspase-3* alleles, 5'-AGGGTCCCATTTGCATAGCTTTGC-3', 5'-GC-GAGTGAGAATGTGCATAAATTC-3', and 5'-TGCTAAAGC-GCATGCTCCAGACTG-3'.<sup>34</sup>

### Hypoxic-Ischemic Injury

Neonatal and adult H/I brain injury was induced in mice on P7 and at 8 weeks of age, respectively, essentially according to the Rice-Vannucci model,<sup>31</sup> with minor modifications.<sup>10</sup> After the mice were deeply anesthetized with isoflurane (2%), the left common carotid artery was dissected and ligated with silk sutures (6/0). After the surgical procedure, the pups and adult mice were allowed to recover for 1 hour. They were then placed in chambers maintained at 37°C through which 8% humidified oxygen (balance, nitrogen) flowed for 40 or 45 minutes (neonate) or 35 or 40 minutes (adult). After hypoxic exposure, the pups and adult mice were returned to their dams and the plastic cages, respectively. The animals were allowed to recover for 3, 8, 24, or 72 hours, or 7 days (neonate). At each stage, brains were processed for biochemical and morphological analyses. This procedure resulted in brain injury in the ipsilateral hemisphere, consisting of cerebral infarction mainly in the hippocampus.<sup>9,13</sup> Control littermates were neither operated on nor subjected to hypoxia.

### Antisera

The preparation of rabbit antibodies against rat LC3<sup>21,37</sup> and Atg7<sup>38</sup> was described previously. Rabbit polyclonal antibodies against ubiquitin (DAKO, Glostrup, Denmark), caspase-3 (Cell Signaling, Danvers, MA), cleaved caspase-3 (Asp175; Cell Signaling), and cleaved caspase-7 (Asp198; Cell Signaling), and mouse monoclonal antibodies against glyceraldehyde-3-phosphate dehydrogenase (GAPDH) (clone 6C5; Ambion, Austin, TX), caspase-7 (clone 10-1-62; BD Biosciences, San Jose, CA), and neuronal nuclei (NeuN) (Chemicon, Temecula, CA) were obtained commercially.

### Sample Preparation for Histochemical and Morphological Analyses

After H/I injury ( $n = 3$  to 5 for each procedure and each stage), mice were deeply anesthetized with pentobarbital (25 mg/kg i.p.) and fixed by cardiac perfusion with 4% paraformaldehyde buffered with 0.1 mol/L phosphate buffer (pH 7.2) containing 4% sucrose for light microscopy and with 2% paraformaldehyde-2% glutaraldehyde buffered with 0.1 mol/L phosphate buffer for ordinary electron microscopy.<sup>21,39,40</sup> For light microscopy, brain tissues were quickly removed from the mice and further immersed in the same fixative for 2 hours at 4°C. Samples processed for paraffin embedding were cut into 5- $\mu$ m sections with a semimotorized rotary microtome (RM2245; Leica, Nussloch, Germany) and placed on silane-coated glass slides. Samples for cryosections were embedded

in OCT compound (Miles, Elkhart, IN) after cryoprotection with 15% and 30% sucrose solutions and cut into 10- $\mu$ m sections with a cryostat (CM3050, Leica). The sections were placed on silane-coated glass slides and stored at -80°C until used. For routine histological studies, paraffin sections or cryosections were stained with hematoxylin and eosin (H&E). Samples for electron microscopy were postfixed with 2% OsO<sub>4</sub> with 0.1 mol/L phosphate buffer, block-stained in 1% uranyl acetate, dehydrated with a graded series of alcohol, and embedded in Epon 812 (TAAB, Reading, UK). For light microscopic observations, semithin sections were cut at 1  $\mu$ m with an ultramicrotome (Ultracut N; Reichert-Nissei, Tokyo, Japan) and stained with toluidine blue. For electron microscopy, silver sections were cut with an ultramicrotome, stained with uranyl acetate and lead citrate, and observed with an electron microscope (H-7100; Hitachi, Tokyo, Japan).

### Immunohistochemical Analyses

For double-immunofluorescent staining, cryosections were first incubated with anti-LC3<sup>21,37</sup> (1:100) or anti-cleaved caspases-3 or -7 (1:100) at 4°C overnight, followed by goat anti-rabbit IgG coupled with Alexa Fluor 488 (Invitrogen, Grand Island, NY) for 1 hour at room temperature. For LC3 detection, further incubations were performed with biotinylated goat anti-rabbit IgG (Vector Laboratories, Burlingame, CA) and finally with streptavidin coupled with Alexa Fluor 488 for 1 hour at room temperature. After immunostaining, terminal dUTP nick-end labeling (TUNEL) staining was performed as described below. The sections were then viewed under a confocal laser-scanning microscope (LSM 5 Pascal; Carl Zeiss, Jena, Germany; or FV1000; Olympus, Tokyo, Japan). For NeuN staining, deparaffinized sections or cryosections were autoclaved for 20 minutes in 10 mmol/L Na-citrate buffer (pH 6.1)<sup>36</sup> before the incubation with NeuN (1:1000). For ubiquitin staining, sections were incubated with anti-ubiquitin (1:1000) without pretreatment. These sections were further incubated with biotinylated goat anti-rabbit or mouse IgG for 1 hour, and finally with peroxidase-conjugated streptavidin (Vector Laboratories) for 1 hour at room temperature. Staining for peroxidase was performed using 0.0125% 3,3'-diaminobenzidine tetrahydrochloride and 0.002% H<sub>2</sub>O<sub>2</sub> in 0.05 mol/L Tris-HCl buffer (pH 7.6) for 10 minutes.

### TUNEL Staining

TUNEL staining was applied to deparaffinized sections or cryosections as previously described.<sup>27,40,41</sup> Briefly, sections with or without a 10-minute proteinase K (20  $\mu$ g/ml) pretreatment at room temperature were incubated with 100 U/ml terminal deoxynucleotidyl transferase (TdT) and 10 nmol/L biotinylated 16-2'-dUTP (Roche Diagnostics, Basel, Switzerland) in TdT buffer (100 mmol/L sodium cacodylate, pH 7.0, 1 mmol/L cobalt chloride, 50  $\mu$ g/ml gelatin) in a humid atmosphere at 37°C for 1 hour, followed by further incubation with Alexa Fluor 594 or peroxidase-conjugated streptavidin (Vector Laborato-

ries) for 1 hour at room temperature. Staining for peroxidase was performed as above. In the case of double-immunofluorescent staining, an *in situ* cell death detection kit, TMR red (Roche Diagnostics), was used according to the manufacturer's recommended protocol after immunohistochemistry.

### Cell Counting

The number of neurons with pyknotic nuclei in sections stained by H&E and that of neurons positive for TUNEL or cleaved caspase-3, or double-positive for TUNEL and cleaved caspase-3 in sections doubly stained for TUNEL and cleaved caspase-3, respectively, were counted in the whole pyramidal regions of the hippocampus located in the same portion (bregma: -1.82 mm of adult C57BL/6J mice<sup>42</sup>) by light microscopy (magnification,  $\times$ 200) (three sections per animal). Data from three animals at each stage were averaged.

### Neuropathological Evaluations

H/I injury and neuroprotection were evaluated by the damaged area and the number of TUNEL-positive (dead) neurons in the pyramidal layers of the hippocampus 3 days after H/I injury using brain sections corresponding to the same portion of the hippocampus as mentioned above. The total and damaged areas in the whole pyramidal layers of the ipsilateral hippocampus from each animal were measured using a morphological analysis software version 2.5 (Mac SCOPE; Mitani Corp., Fukui, Japan). The damaged area was defined as a region of the pyramidal layers that was NeuN-negative (see Figure 7D). The degree of H/I injury 3 days after ischemic insult was classified into four grades: the number of TUNEL-positive neurons in the pyramidal layers of the hippocampus per section was less than 10 for grade 0, 11 to 100 for grade I, 101 to 200 for grade II, and more than 201 for grade III. The percentage of mice showing each grade was further calculated in the cases of Atg7-deficient mice ( $n = 17$ ) and their littermate controls ( $n = 32$ ). The damaged area in the hippocampal pyramidal layers was also examined 7 days after H/I injury, in which time clear-cut shrinkage occurred in the ipsilateral hippocampus of control littermate mice (Atg7<sup>flx/flx</sup> mice), resulting in loss of ipsilateral hippocampal areas. To quantitate these damaged areas after neonatal HI, the areas of lesioned and unlesioned hippocampi were measured and compared within the same section, using the same software as mentioned above.<sup>13</sup> The area loss of the lesioned ipsilateral hippocampus was calculated as a percentage of the intact contralateral hippocampus and the area loss was determined for each animal by measurement of at least three sections according to the method mentioned above. The degree of hippocampal damage was measured using Atg7-deficient ( $n = 11$ ) and their littermate control ( $n = 12$ ) mice.

### Sample Preparations for Biochemical Analyses

Anesthetized mice were sacrificed by decapitation at 3, 8, 24, or 72 hours after H/I injury ( $n = 5$  per group), and untreated control animals were sacrificed on P7 or at 8 weeks ( $n = 6$  per group). The brains were rapidly dissected on a bed of ice. The left and right hippocampi were separately excised from the mice, frozen in liquid nitrogen, and stored at  $-80^{\circ}\text{C}$  until used.

### Analysis of DNA Fragmentation

Genomic DNA was isolated according to a previously described method.<sup>40</sup> Briefly, each tissue was separately homogenized gently in 1 ml of a lysis buffer consisting of 4 mol/L guanidine thiocyanate and 0.1 mol/L Tris-HCl, pH 7.0, and incubated at room temperature for 1 hour. Then, 20  $\mu\text{l}$  of QIAEX II suspension (Qiagen, Hilden, Germany) was added to each sample, and the samples were vortexed, incubated at room temperature for 1 hour, and finally spun at  $12,500 \times g$  for 2 minutes. The pellets were washed by resuspending them three times in a NEW Wash solution (GENECLEAN kit; Bio 101, Vista, CA) consisting of 50% ethanol, 100 mmol/L NaCl, 10 mmol/L Tris/HCl, and 1 mmol/L ethylenediaminetetraacetic acid, pH 7.5, followed by resuspension in a TE buffer consisting of 10 mmol/L Tris/HCl and 1 mmol/L ethylenediaminetetraacetic acid, pH 8.0. Samples were incubated at room temperature for 10 minutes and spun at  $12,500 \times g$  for 2 minutes. The supernatants were collected and stored at  $-30^{\circ}\text{C}$  until used.

To visualize DNA laddering in DNA samples from individual animals, a ligation-mediated polymerase chain reaction (LMPCR) was performed with some modifications, as outlined.<sup>43,44</sup> Briefly, two unphosphorylated oligonucleotides (24 bp, 5'-AGCACTCTCGAGCCTCTCACCGCA-3'; 12 bp, 5'-TGCGGTGAGAGG-3') were synthesized (Invitrogen). These are DNA fragments that are never amplified from normal mouse brain DNA. The oligonucleotides were annealed by heating to  $55^{\circ}\text{C}$  for 10 minutes, and the mixture was allowed to cool to  $10^{\circ}\text{C}$  for 55 minutes in advance of the experiment. Genomic DNA (1.0  $\mu\text{g}$ ) was mixed with 1 nmol each of the 24-bp and 12-bp unphosphorylated oligonucleotides in 50  $\mu\text{l}$  of T4 DNA ligase buffer (Promega, Madison, WI) and 3 U of T4 DNA ligase (Promega). The mixture was incubated at  $16^{\circ}\text{C}$  overnight, and the samples were then diluted with TE to a final concentration of 5 ng/ $\mu\text{l}$ , and stored at  $-20^{\circ}\text{C}$  until used for PCR. The 24-mer adaptor also served as a primer in the LMPCR (50  $\mu\text{l}$  volume), in which 25 ng of ligated DNA was amplified with reagents from the Expand high-fidelity PCR system (Roche) under the following conditions: hot start ( $72^{\circ}\text{C}$  for 8 minutes) with 1.75 U Expand high-fidelity enzyme mix (TaqDNA polymerase and Tgo DNA polymerase) added after 3 minutes, 20 (neonate) or 25 (adult) cycles ( $94^{\circ}\text{C}$  for 1 minute,  $72^{\circ}\text{C}$  for 3 minutes), and postcycling ( $72^{\circ}\text{C}$  for 15 minutes). The amplified DNA was separated by electrophoresis on a 2% agarose gel, visualized by staining with ethidium bromide, and photographed on a UV transilluminator (Bio-Rad, Hercules, CA).

### Immunoblot Analysis

Each tissue was independently homogenized in a lysis buffer [1% Triton X-100 and 1% Nonidet P-40 in phosphate-buffered saline (PBS)] containing a protease inhibitor cocktail (Nacalai, Kyoto, Japan). After two centrifugations at  $10,500 \times g$  for 10 minutes each at  $4^{\circ}\text{C}$ , the protein concentrations in the supernatants were determined using the BCA protein assay system (Pierce, Rockford, IL) and used for immunoblotting. The samples (15  $\mu\text{g}$  for the detection of LC3 or GAPDH, 40  $\mu\text{g}$  for Atg7, or for caspases-3 and -7) were then analyzed by 12.5% sodium dodecyl sulfate-polyacrylamide gel electrophoresis. The electrophoretic transfer of proteins from polyacrylamide gels to a polyvinylidene difluoride membrane (Immobilon-P; Millipore Co., Bedford, MA) was performed according to the method of Towbin and colleagues.<sup>45</sup> The sheets were soaked in PBS containing 0.1% Tween 20 and 5% bovine serum albumin (Sigma, St. Louis, MO) to block nonspecific binding, and then incubated overnight with anti-LC3 (1:1000), anti-GAPDH (10 ng/ml), anti-Atg7 (1  $\mu\text{g}/\text{ml}$ ), anti-caspase-3 (1:1000), anti-caspase-7 (1:1000), or anti-cleaved caspase-7 (1:1000). The membranes were washed three times for 10 minutes in PBS containing 0.1% Tween 20 and then further incubated for 1 hour at room temperature with horseradish peroxidase-labeled secondary antibody (pig anti-rabbit or goat anti-mouse IgG, DAKO) diluted 1:1000. After three 10-minute washes in PBS with 0.1% Tween 20, the membranes were treated with Immobilon Western chemiluminescent horseradish peroxidase substrate (Millipore Co.) for 2 minutes and then observed using an LAS-3000 mini system (Fuji Photo Film, Tokyo, Japan). Immunoreactive bands were quantified using the Image Gauge software (Fuji Photo Film). Based on the optical density of the different bands in individual animals ( $n = 3$  for each stage) LC3-II/LC3-I ratio was calculated. As a reference of caspase-7 activation, primary mouse hepatocytes that were isolated according to the method as described previously<sup>46</sup> and treated with tumor necrosis factor- $\alpha$  (25 ng/ml) (R&D Systems, Minneapolis, MN) and actinomycin D (0.2  $\mu\text{g}/\text{ml}$ ) (Sigma) for 6 hours were used, and their lysates were subjected to Western blotting.

### Measurement of DEVDase (Caspases-3 and -7) Activity

The DEVD-AMC cleavage assay in hippocampal tissue was performed as described elsewhere.<sup>40,44</sup> Briefly, each tissue was independently homogenized in 100  $\mu\text{l}$  of lysis buffer containing 10 mmol/L HEPES, pH 7.5, 42 mmol/L KCl, 5 mmol/L  $\text{MgCl}_2$ , 1 mmol/L dithiothreitol, 0.5% CHAPS, 1 mmol/L phenylmethyl sulfonyl fluoride, and a protease inhibitor cocktail, and spun at  $10,500 \times g$  for 15 minutes at  $4^{\circ}\text{C}$ . Tissue lysates (10  $\mu\text{l}$  each) were incubated in an opaque 96-well plate with 190  $\mu\text{l}$  of assay buffer (25 mmol/L HEPES, 1 mmol/L ethylenediaminetetraacetic acid, 3 mmol/L dithiothreitol, 0.1% CHAPS, 10% sucrose, and a protease inhibitor cocktail) containing 30  $\mu\text{mol}/\text{L}$  of the following substrate; *N*-acetyl-Asp-Glu-Val-

Asp-AMC (for caspases-3 and -7) (Peptide Institute, Inc., Minoo, Japan). The fluorescence intensity (excitation, 365 nm; emission, 465 nm) was monitored using a Spectramax microtiter plate reader (Molecular Devices, Sunnyvale, CA). The accumulation of fluorescence was linear for at least 45 minutes. Protein concentrations in each lysate were determined by BCA protein assay, as described above. The experiments were repeated three times with samples from each hippocampus, and the data from three animals in each group were averaged.

### Statistical Analysis

Ratios (%) of the damaged areas to the total areas in the ipsilateral hippocampal pyramidal layers in Atg7-deficient ( $n = 17$ ) and littermate control ( $n = 32$ ) mice 3 days after H/I injury and the area loss (%) of the lesioned ipsilateral hippocampus that was calculated as a percentage of the intact contralateral hippocampus in Atg7-deficient ( $n = 11$ ) and their littermate control ( $n = 12$ ) mice 7 days after H/I injury, respectively, were compared using the Mann-Whitney *U*-test. Differences between two groups were assessed using two-tailed Student's *t*-tests. Data were expressed as mean  $\pm$  SD. We assumed statistically significant differences at  $P < 0.05$ .

### Results

#### Presence of Caspase-Dependent and -Independent Neuron Death in the Hippocampus after H/I Injury

Because the hippocampus has been shown to be the most vulnerable to ischemic insult,<sup>9,13</sup> we focused on the damage in the pyramidal regions of the hippocampus in neonatal and adult mouse brains after H/I injury and first re-examined the pathways that were involved in H/I injury-induced pyramidal neuron death in the neonatal hippocampus. In control neonatal mice at P7, hippocampal pyramidal neurons with pyknotic nuclei were hardly detected (Figure 1A), although positive staining for cleaved caspase-3 was demonstrated in a small number of pyramidal neurons with positive TUNEL staining in nuclei (Figure 1F). Such neuron death was naturally occurring cell death (programmed cell death) that has been shown in the hippocampus of mouse brains around P7.<sup>47</sup> Damaged neurons after H/I injury were detected only in the ipsilateral hippocampus,<sup>9,13</sup> whereas neurons in the contralateral hippocampus appeared histologically intact could not be distinguished from those in the untreated control brains (data not shown). In an H/I injury model using wild-type neonatal mice, we confirmed that the death mode of pyramidal neurons in the hippocampus was distinct from necrosis (Figure 1, B–D, G–J, and M); ~35% of pyramidal neurons in the hippocampus were immunostained for activated caspase-3 8 hours after H/I injury (Figure 1, H and M). DEVDase activity was increased in the ipsilateral hippocampus 8 hours after H/I injury, whereas the cleaved form of caspase-3, but not

caspase-7, was clearly detected in the tissue by Western blotting (Figure 1, N and O). By immunostaining, however, cleaved caspase-7-positive neurons appeared in the ipsilateral hippocampus after H/I injury, but they were rare (Figure 1, K and L; Figure 3C). The number of TUNEL-positive neurons increased at 24 and 72 hours, although the number of pyknotic neurons was already augmented 8 hours later (Figure 1M). These data indicate that both caspase-3-dependent and caspase-3-independent pyramidal neuron death occurred in the neonatal hippocampus after H/I injury.

#### Caspase-Independent Pyramidal Neuron Death in the Hippocampus after H/I Injury Is Accompanied by DNA Fragmentation into Oligonucleosomes

To confirm further the presence of caspase-independent neuron death in the neonatal hippocampus after H/I injury, we used caspase-3-deficient and CAD-deficient mice.<sup>33–35,48</sup> Genomic DNA fragmentation into oligonucleosomes is one of the hallmarks of apoptotic cell death and is mediated by CAD.<sup>49</sup> Because programmed cell death occurred around P8<sup>47</sup> (Figure 1F), the genomic DNA from the untreated hippocampus of neonatal brains was weakly but distinctly fragmented into oligonucleosomes, as evidenced by an LMPCR method (Figure 2D, lane 1)<sup>43</sup> DNA laddering occurred intensely in the ipsilateral side and weakly in the contralateral side of wild-type neonatal hippocampi after H/I injury (Figure 2D, lanes 2 and 3). Using CAD-deficient neonatal mice,<sup>33</sup> we examined H/I injury-induced alterations in hippocampal pyramidal neurons and found that the degree of damage was similar to that in the wild-type mice 24 hours later (Figure 2, A and C). In this situation, DNA laddering was detectable in the ipsilateral hippocampus (Figure 2D, lane 7), indicating that nuclear DNA in the damaged neurons was fragmented by a DNase other than CAD. Moreover, no DNA laddering was observed in the contralateral hippocampus (Figure 2D, lane 6), suggesting that the DNA fragmentation of programmed neuron death is mediated in the wild-type neonatal hippocampus by CAD. As has been shown in caspase-3-deficient mice,<sup>44</sup> H/I induced changes such as the appearance of shrunken neurons with pyknotic nuclei were abundant in each pyramidal layer of the hippocampus within 24 hours after H/I injury (Figure 2B; Figure 3, D and E). It has been suggested that long-term inhibition of caspase-3 during development by its genetic ablation up-regulates caspase-3-independent cell death pathways and increases the vulnerability of the developing brain to neonatal H/I injury.<sup>44</sup> However, the DNA fragmentation in the ipsilateral and contralateral hippocampi of caspase-3-deficient mouse brains after H/I injury occurred similar to that in the wild-type mouse brains (Figure 2D, lanes 4 and 5). Because DNA laddering did not appear in the contralateral side of the CAD-deficient hippocampus after H/I injury, it is assumed that the DNA laddering detected in the contralateral side of the caspase-3-deficient hippocampus was mediated by

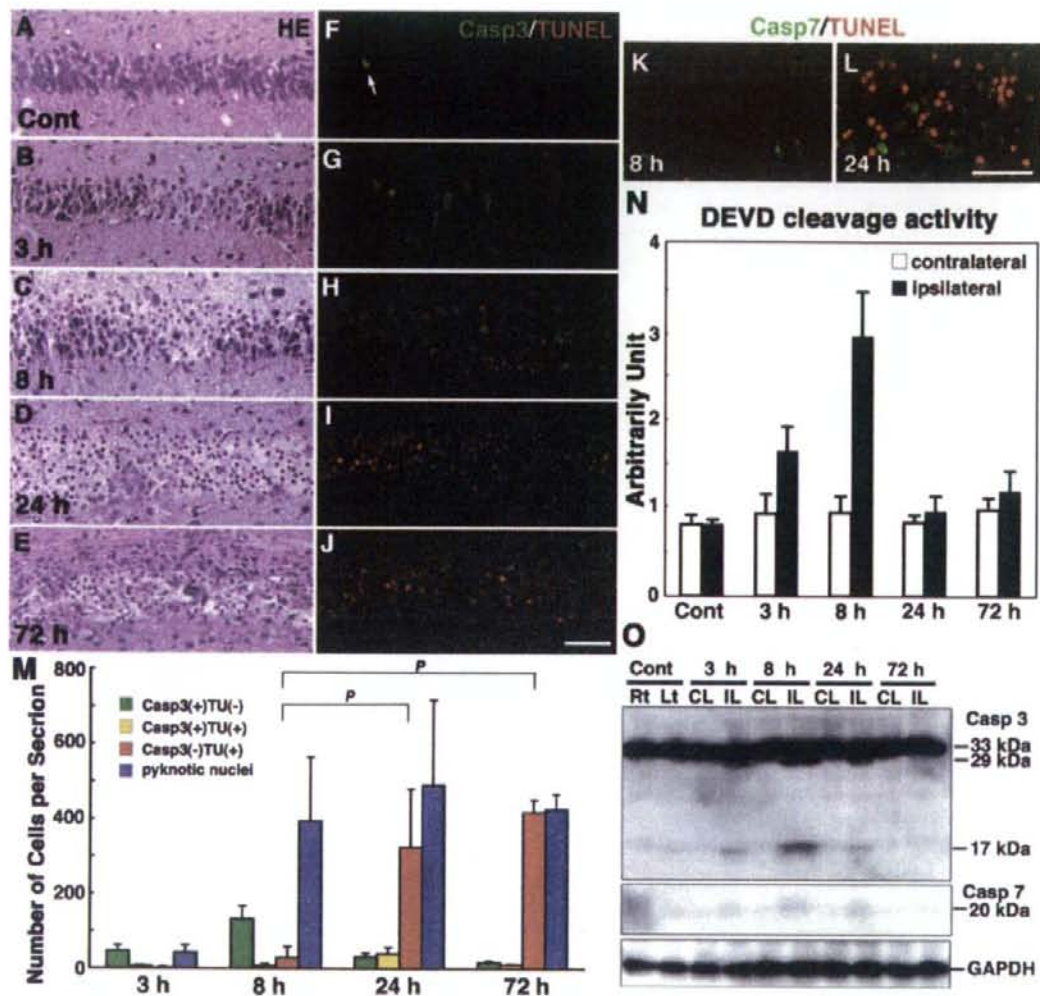


**Figure 1.** Activation of caspases and TUNEL staining in the hippocampus of wild-type neonatal mice after H/I injury. **A–J:** Histological sections of the left hippocampus of an untreated control (Cont) mouse at P7 (**A, F**) and ipsilateral hippocampus obtained 3 (**B, G**), 8 (**C, H**), 24 (**D, I**), and 72 hours (**E, J**) after H/I injury and stained with H&E (**A–E**) or for TUNEL and the active form of caspase-3 (**F–J**). An arrow in **F** shows a cleaved caspase-3-positive neuron undergoing programmed cell death. **K and L:** Double staining for TUNEL and the cleaved form of caspase-7 in the ipsilateral hippocampus at 8 (**K**) and 24 (**L**) hours after H/I injury. **M:** Number of neurons with pyknotic nuclei stained by H&E and the number of neurons positive for the active form of caspase-3 (Casp3), TUNEL (TU), or both in the pyramidal layers per hippocampal section at 3, 8, 24, and 72 hours after H/I injury. Counts were taken from three sections per animal, and the final value presented is the mean  $\pm$  SD for three animals.  $P < 0.001$ . **N:** Proteolytic activity of the DEVDase for caspases-3 and -7 in the ipsilateral and contralateral hippocampus 3, 8, 24, and 72 hours after H/I injury. The activity in the contralateral hippocampus was used as control. The final value presented is the mean  $\pm$  SD for three animals. **O:** The cleavage of caspases-3 and -7 in the contralateral (CL) and ipsilateral (IL) hippocampi of wild-type neonatal mouse brains at 3, 8, 24, and 72 hours after H/I injury. Hippocampal tissues of the right (Rt) and left (Lt) sides from untreated neonatal mice were used as controls. Scale bars = 50  $\mu$ m.

CAD. It has been shown that caspase-7, which is structurally and functionally similar to caspase-3, compensates for the lack of caspase-3.<sup>48,50</sup> In fact, cleaved caspase-7 was demonstrated in pyramidal neurons with 4,6-diamidino-2-phenylindole (DAPI)-stained shrunken nuclei in the contralateral hippocampus deficient in caspase-3 (Figure 3A). More interestingly, this cleaved caspase-7 was shown in numerous pyramidal neurons of the ipsilateral hippocampus after H/I injury by immuno-

histochemistry and in the ipsilateral hippocampus by Western blotting, although its immunoreactivity was somewhat weak (Figure 3, E and F). These results suggest that CAD that was activated by caspase-7 may be involved in the DNA ladder formation in caspase-3-deficient hippocampi after H/I injury. Furthermore, it has been shown by electron microscopy that small patches of chromatin clumping appear in the nuclei of pyramidal neurons in neonatal mice after H/I injury (Figure 2E).<sup>7</sup> In

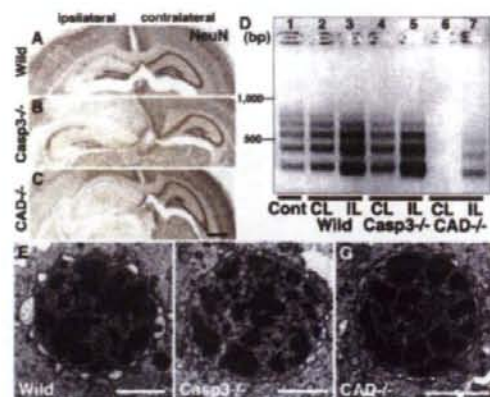


**Figure 2.** Pyramidal neuron death in the hippocampus of neonatal mouse brains after H/I injury. **A–C:** Coronal histological sections of wild-type (Wild) (A), caspase-3-deficient (Casp3<sup>-/-</sup>) (B), and CAD-deficient (CAD<sup>-/-</sup>) (C) brains including ipsilateral and contralateral hippocampi 24 hours after H/I injury. Staining with NeuN. **D:** Genomic DNA fragmentation detected by LMPER. Samples were obtained from the hippocampus of an untreated wild-type brain (Cont) (lane 1), and the contralateral (CL) and ipsilateral (IL) hippocampi of wild-type (lanes 2 and 3), caspase-3-deficient (lanes 4 and 5), and CAD-deficient (lanes 6 and 7) brains 24 hours after H/I injury. **E–G:** A nucleus with small patches of chromatin clumping was observed in the pyramidal neurons of not only wild-type (E) but also caspase-3-deficient (F) and CAD-deficient (G) mouse hippocampi 8 hours after H/I injury. Scale bars: 500  $\mu$ m (C); 2  $\mu$ m (E–G).

the cases of caspase-3- and CAD-deficient mice, such chromatin clumping was also detected in pyramidal neurons within 24 hours after H/I injury (Figure 2, E and F). Collectively, these data suggest that neuron death in the pyramidal layers of the neonatal mouse hippocampus after H/I injury is mediated by both caspase-3-dependent and -independent pathways, in the latter of which the genomic DNA is weakly fragmented into oligonucleosomes by a DNase other than CAD.

#### Induction of Autophagy in Pyramidal Neurons of the Neonatal Hippocampus after H/I Injury

Although it is generally accepted that autophagy is essential for the maintenance of cellular metabolism and survival,<sup>16–18</sup> it has also been demonstrated to be involved in cell death.<sup>19,25,26,51</sup> To understand further whether autophagy is involved in hippocampal pyramidal neuronal damages after H/I injury, we examined alterations in amounts of LC3, a marker of autophagy.<sup>29</sup> As shown in Figure 4, A and B, the amount of LC3-II increased in the ipsilateral and contralateral hippocampi of wild-type neonatal mice after the H/I insult, whereas the ratios of the amounts of LC3-II to LC3-I were significantly higher in the ipsilateral side of neonatal hippocampi at each time point than in the contralateral side and also than in the untreated control hippocampi. This tendency was also confirmed by double staining for LC3 and DAPI: intense LC3 staining appeared granular in the perikaryal region of pyramidal neurons in the hippocampus of the damaged side at 3, 8, and 24 hours (Figure 4, C, E, and G; Supplemental Figure 1 see <http://ajp.amjpathol.org>),

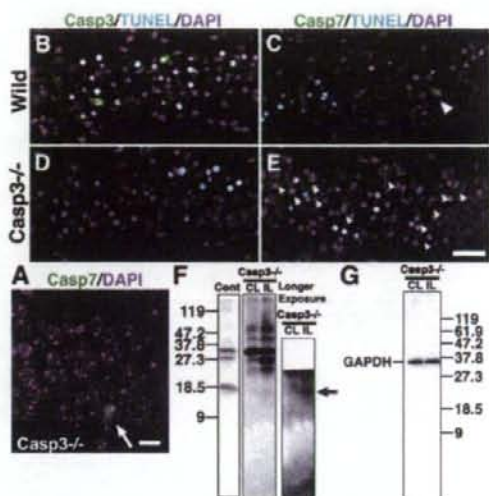


**Figure 3.** H/I injury-induced pyramidal neuron death in the hippocampi of wild-type and caspase-3-deficient neonatal mouse brains. **A:** Double staining of cleaved caspase-7 (Casp7) and DAPI in the contralateral hippocampus of a caspase-3-deficient mouse brain 8 hours after H/I injury. An arrow shows a cleaved caspase-7-positive neuron. **B–E:** Triple staining of cleaved caspase-3 (B, D) or cleaved caspase-7 (C, E), TUNEL, and DAPI in the ipsilateral hippocampi of wild-type (Wild) (B, C) and caspase-3-deficient (D, E) neonatal mouse brains 8 hours after H/I injury. **F and G:** The cleavage of caspase-7 (F) and GAPDH (G) in the contralateral (CL) and ipsilateral (IL) hippocampi of caspase-3-deficient mouse brains 8 hours after H/I injury. In the ipsilateral hippocampus of a caspase-3-deficient mouse brain, a cleaved form appears intensely at ~27 kDa but not at 18 kDa (F, middle), whereas an activated form of caspase-7 can be detected at ~18 kDa under a longer exposure (F, right). These cleaved forms, along with the proform of caspase-7, correspond with those detected in a control lane (Cont) showing primary hepatocytes treated with tumor necrosis factor- $\alpha$  and actinomycin D for 6 hours (F, left). Scale bars: 10  $\mu$ m (A); 30  $\mu$ m (E).

whereas the pyramidal neurons in the contralateral side showed only weak staining for LC3 in the neuronal perikarya at the corresponding time points (Figure 4, D, F, and H; Supplemental Figure 1 see <http://ajp.amjpathol.org>). As evidenced by DAPI staining, the pyramidal neurons, in which granular immunodeposits for LC3 abundantly appeared in the ipsilateral side, frequently possessed shrunken or irregularly shaped nuclei with condensed or clumped chromatin (Figure 4, C, E, and G; Supplemental Figure 1 see <http://ajp.amjpathol.org>), indicating that such damaged neurons were mostly dying. Electron microscopic observations showed that neurons in the ipsilateral pyramidal layer of the neonatal hippocampus after H/I injury contained abundant autophagic vacuoles from an early stage, some of which were nascent autophagosomes with double-membrane structures (Figure 4, I and K). Such neurons also frequently contained nuclei with small patches of clumped chromatin (Figure 4I). These degenerating neurons increased in number with time after the H/I insult. As far as we observed hippocampal pyramidal neurons in the contralateral side after H/I injury, there were no neurons that possessed nuclei with small patches of chromatin clumping and autophagic vacuoles in the perikaryal region at any time examined (Supplemental Figure 2 see [- 343 -](http://</a></p>
</div>
<div data-bbox=)

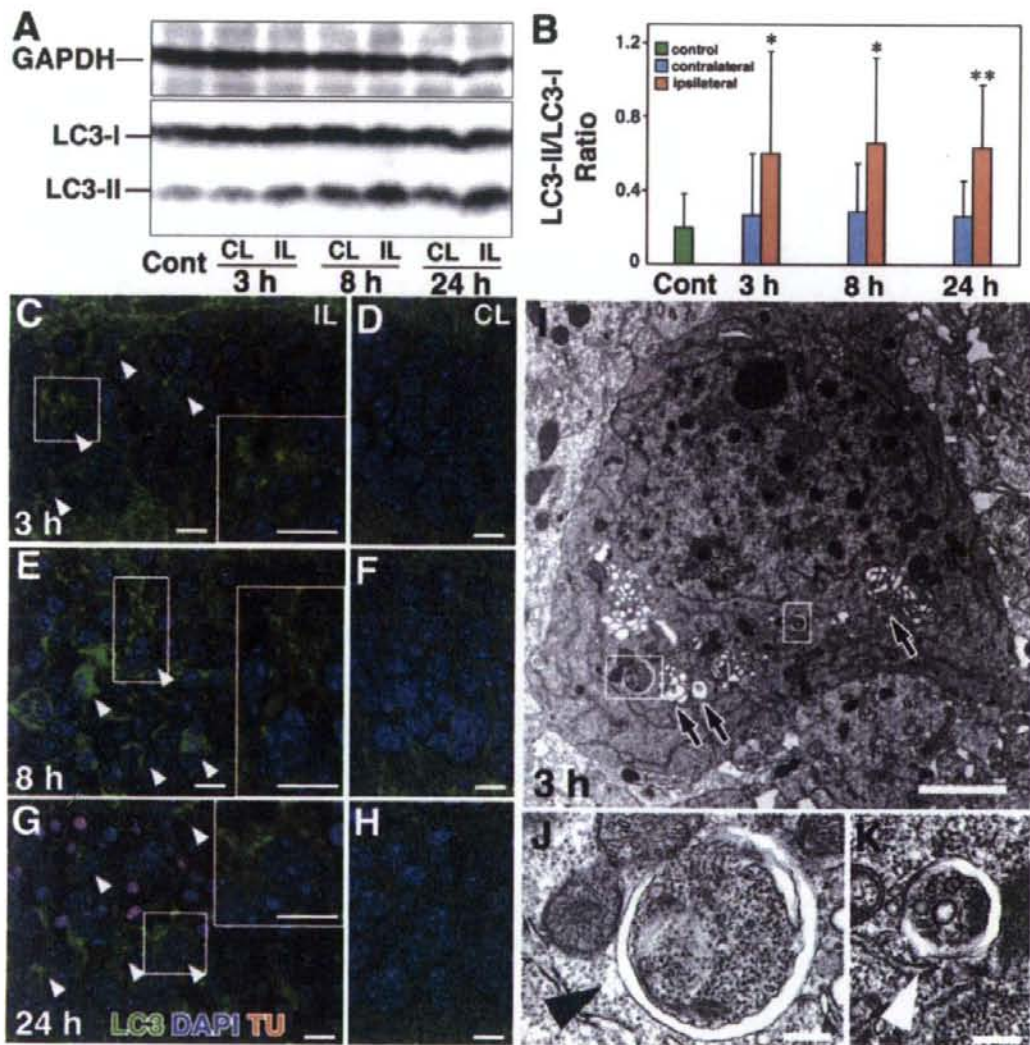


**Figure 4.** H/I injury induces autophagy in the hippocampi of wild-type neonatal mouse brains. **A:** Western blotting of LC3 in the untreated hippocampus (Cont) and the ipsilateral (IL) and contralateral (CL) hippocampi of neonatal mouse brains at 3, 8, and 24 hours after H/I injury. **B:** Quantification of **A**. The ratios of the amounts of LC3-II to LC3-I were calculated at each corresponding time. The final values represent the mean  $\pm$  SD for three animals. \* $P < 0.05$  and \*\* $P < 0.01$  (Student's *t*-test) for the comparison of the values between the ipsilateral and contralateral sides. **C–H:** Triple staining of LC3, TUNEL (TU), and DAPI in the ipsilateral (**C, E, G**) and contralateral (**D, F, H**) hippocampi of neonatal mouse brains 3 (**C, D**), 8 (**E, F**) and 24 (**G, H**) hours after H/I injury. Intense granular staining for LC3 is indicated by **arrowheads**, and granular staining of LC3 in **boxed areas** are shown in **insets** (**C, E, G**). **I–K:** Electron micrographs of a CA1 pyramidal neuron in the hippocampi of wild-type neonatal mouse brains 3 hours after H/I injury. Abundant vacuolar structures (**I, arrowheads**) and nascent autophagosomes (**I, boxed areas**) (**J** and **K, arrowheads**) were detected in the perikarion. Scale bars: 10  $\mu$ m (**A–H**); 3  $\mu$ m (**D**); 0.5  $\mu$ m (**J, K**).

*ajp.amjpathol.org*). Along these lines, however, dying neurons with typical apoptotic figures such as small nuclei with typical chromatin condensation and shrinkage of cell bodies could be detectable but were small in number (data not shown), reflecting the presence of programmed cell death at this postnatal period.<sup>47</sup> These results suggest that autophagy is strongly induced in the neurons undergoing death in the pyramidal layer of the neonatal hippocampus after H/I injury.

Induction of autophagy after H/I injury was also shown in pyramidal neurons of the hippocampus deficient in caspase-3 or CAD, as evidenced by immunohistochemistry and electron microscopy (Figure 5). As in wild-type neonatal mice, LC3 immunoreactivity was punctate in ipsilateral pyramidal neurons of the mutant mouse hippocampi after H/I injury (Figure 5, **A** and **C**; Supplemental Figure 1 see <http://ajp.amjpathol.org>). Electron microscopic observations showed that autophagic vacuoles



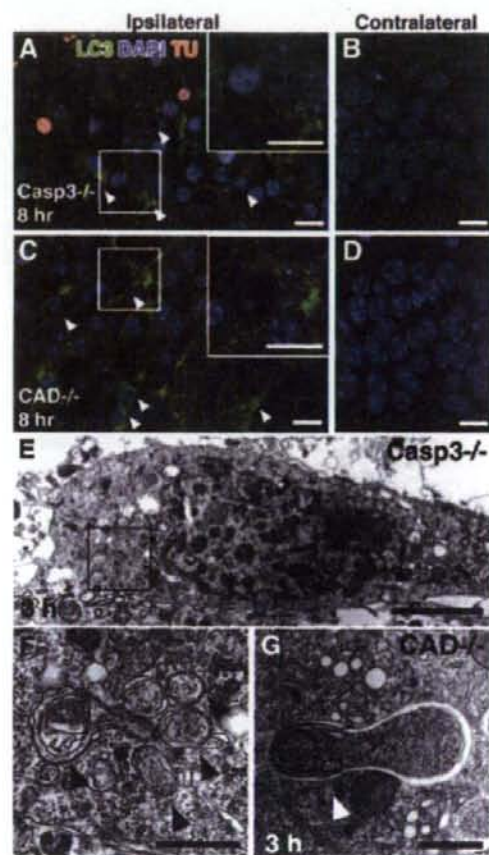


**Figure 5.** Induction of autophagy in the hippocampus of neonatal mutant mouse brains after H/I injury. **A–D:** Triple staining of LC3, TUNEL (TU), and DAPI in the CA1 pyramidal layer of ipsilateral (**A, C**) and contralateral (**B, D**) hippocampi deficient in caspase-3 ( $Casp3^{-/-}$ ) (**A, B**) and CAD ( $CAD^{-/-}$ ) (**C, D**), respectively, 8 hours after H/I injury. Intense granular staining for LC3 is indicated by **arrowheads**, and granular staining of LC3 in **boxed areas** are shown in **insets** (**A, C**). **E–G:** Electron micrographs of pyramidal neurons of the hippocampus in mice deficient in caspase-3 (**E, F**) and CAD ( $CAD^{-/-}$ ) (**G**) obtained 3 hours after H/I injury. **E** and **F:** Pyramidal neuron containing vacuolar structures in the perikaryal region and showing numerous patches of chromatin clumping in the nucleus (**E**). Nascent autophagosomes that contained part of the cytoplasm and wrapped by endoplasmic reticulum-like tubular structures were abundantly observed in the **boxed area** of **E** (**arrowheads** in **F**). **G:** Part of the perikaryal area of a pyramidal neuron of the hippocampus in a CAD-deficient mouse showing a nascent autophagosome wrapped by an endoplasmic reticulum-like tubule (**arrowhead**). Scale bars: 10  $\mu$ m (**A–D**); 3  $\mu$ m (**E**); 1  $\mu$ m (**F** and **G**).

with single- or double-membrane structures abundantly appeared in the perikaryal region of the pyramidal neurons in the hippocampus of caspase-3- or CAD-deficient mouse brains after H/I injury (Figure 5, E–G), whereas dense chromatin profiles in nuclei of these neurons were similar to those detected in nuclei of wild-type pyramidal neurons after H/I injury (Figure 5E). The results also confirmed that autophagy is highly induced in the damaged pyramidal neurons of the ipsilateral hippocampus in caspase-3- and CAD-deficient mouse brains after H/I injury.

### Inhibition of H/I Induced-Neuron Death in the Neonatal Hippocampus by Atg7 Deficiency

We next investigated whether autophagy directly participates in the death of hippocampal pyramidal neurons after H/I insult, using mice that lack Atg7 specifically in the central nervous system (CNS) ( $Atg7^{lox/lox}$ ; nestin-Cre).<sup>36</sup> Atg7 functions as an E1 enzyme in the Atg conjugation system and together with Atg3, an E2 enzyme, conjugates phosphatidyl ethanolamine to the C-terminal glycine residue of LC3-I, forming the membrane-bound form, LC3-II.<sup>52</sup> Mice with an Atg7-deficiency in the CNS exhibit behavioral deficits and die at ~8 weeks of age. Massive neuronal loss occurs in the cerebral and cerebellar cortices of these mutant mice, and inclusion bodies composed of polyubiquitinated proteins start to accumulate in the neurons at ~3 weeks of age.<sup>36</sup> To be certain that potential baseline CNS abnormalities in *Atg7*-mutant neonatal mice would not influence our results, we morphologically evaluated their CNS tissue from birth to 2 weeks of age, encompassing the experimental period of this study. Histological sections from *Atg7* mutant mouse brains showed an intact, architecturally normal hippocampus, exhibiting no ubiquitin-positive inclusion bodies within neurons until after 2 weeks of life (Supplemental Figure 3, A–D, see <http://ajp.amjpathol.org>).

As expected, no Atg7 was detectable in the hippocampus of the CNS of *Atg7*-deficient mice; mice showed no conversion of LC3-I to LC3-II in the ipsilateral and contralateral hippocampi at P8, 1 day after H/I injury, by Western blotting, but Atg7 expression and conversion of LC3-I to LC3-II were normal in the hippocampi from control littermate brains (Supplemental Figure 3, E and F, see <http://ajp.amjpathol.org>). When the *Atg7*-deficient mice were subjected to H/I injury at P7 and neuronal morphology was assessed by histological analysis, TUNEL staining, and NeuN immunohistochemistry, 13 of 17 mice (76%) showed no pyknotic nuclei or positive TUNEL staining in the hippocampus 3 days later (Figure 6, A, C, E, and G). In contrast, only 22% of the littermate control mice (7 of 32 mice) escaped damage to the pyramidal neurons, and the rest had severely damaged hippocampal neurons (Figure 6, B, D, F, and H). For a more quantitative evaluation, the degree of damage 3 days after H/I injury was examined by measuring the ratio of the damaged areas to the total area of the pyramidal layer in the hippocampus (Figure 6I). The median value in *Atg7*-deficient mice (0.32) was significantly lower than that in littermate control mice (27.38) ( $P < 0.001$ ). In addition, the degree of damage was also analyzed by subcategorizing severity of damage into four groups (0 to III). Among the *Atg7*-deficient brains, all but four were grade 0, and of these four, two each were grade I and grade II. By contrast, 9% of the control littermate brains showed damage at grade I, 9% at grade II, and 59% at grade III (Figure 6J).

It has been shown that delayed neuronal death occurs in the pyramidal layers of the hippocampus and damaged pyramidal layers are replaced by glial cells within 7 days after ischemic insult.<sup>13</sup> To exclude the possibility that the inhibition of autophagy simply delayed the onset

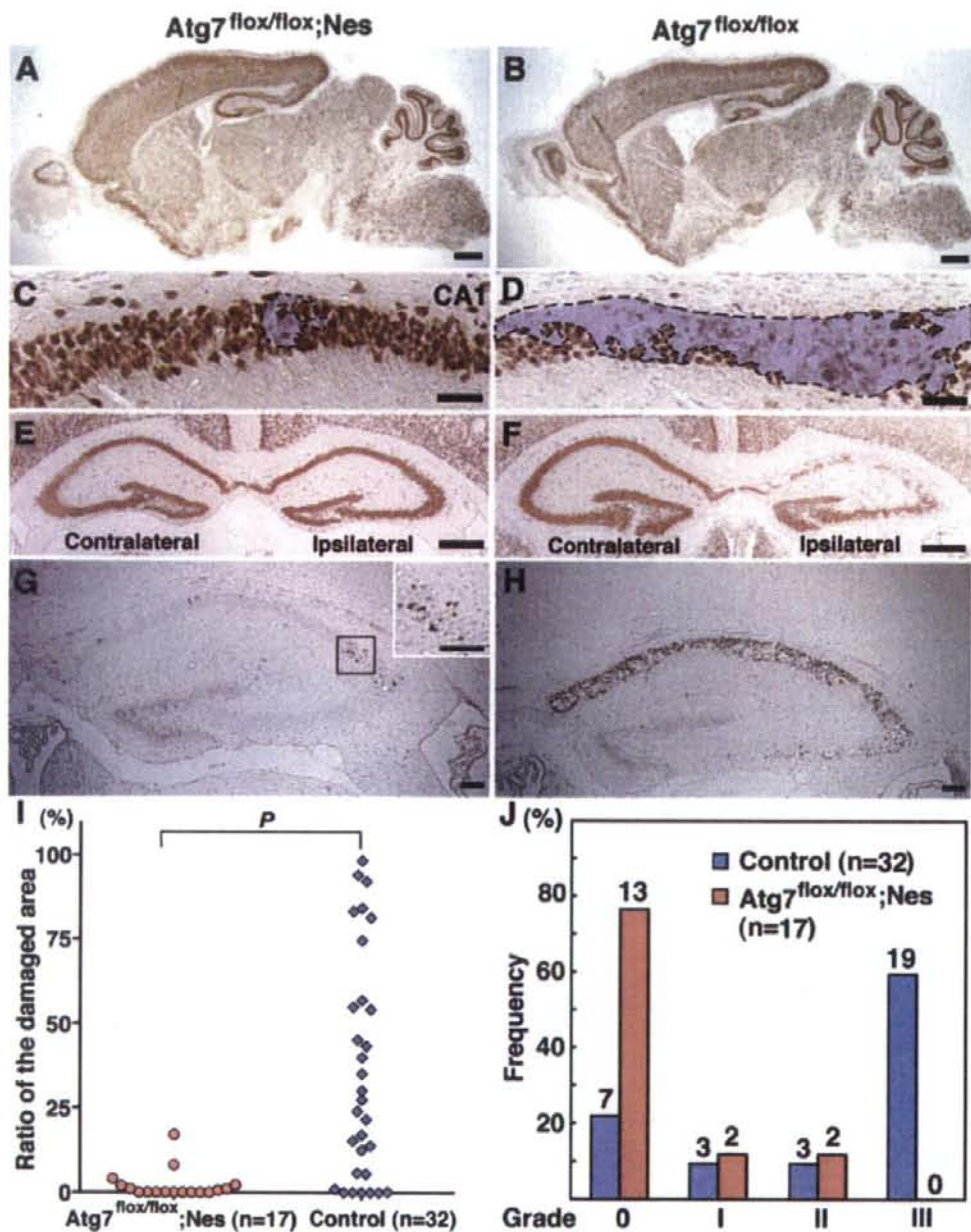


**Figure 6.** *Atg7* deficiency prevents neuron death in the hippocampus of neonatal mouse brains 3 days after H/I injury. **A–H:** Sagittal (**A–D**) and frontal (**E–H**) sections of the *Atg7*-deficient mouse brains (*Atg7<sup>flox/flox</sup>;Nes*) in the CNS (**A, C, E, G**) and its littermate (*Atg7<sup>flox/flox</sup>*) (**B, D, F, H**) 3 days after H/I injury. NeuN (**A–F**) and TUNEL (**G, H**) staining. Damaged areas in **A** and **B** are shown in **C** and **D** and encircled by broken lines. **I** and **J:** Evaluation of damaged areas. **I:** Ratios (%) of damaged areas to the total areas in the hippocampal layers of *Atg7*-deficient ( $n = 17$ ) and littermate control ( $n = 32$ ) mouse brains 3 days after H/I injury.  $P < 0.001$  (Mann-Whitney  $U$ -test for the comparison of the median values between the two groups). **J:** Incidence of hippocampal damage 5 days after H/I injury. The severity of the H/I injury was graded according to the number of TUNEL-positive neurons in the pyramidal layers of the hippocampus per section (less than 10 for grade 0, 11 to 100 for grade I, 101 to 200 for grade II, and more than 201 for grade III). The percentage of mice classified into each grade was determined from 17 *Atg7<sup>flox/flox</sup>;nestin-Cre* (*Atg7<sup>flox/flox</sup>;Nes*), and 32 control littermate (*Atg7<sup>flox/flox</sup>*) mice. The number of mice belonging to each grade was described in the top of each bar. Scale bars: 500  $\mu\text{m}$  (**A, B, E, F**); 50  $\mu\text{m}$  (**C, D**); 100  $\mu\text{m}$  (**G, H**, inset of **G**).

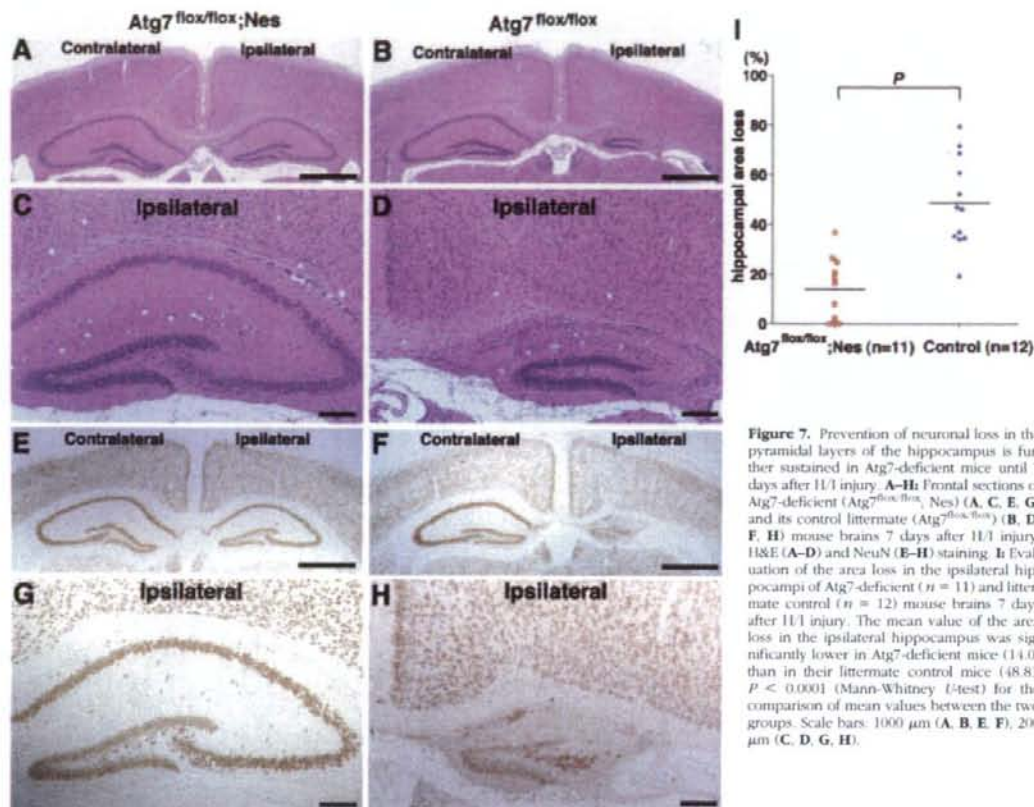


**Figure 7.** Prevention of neuronal loss in the pyramidal layers of the hippocampus is further sustained in Atg7-deficient mice until 7 days after H/I injury. **A–H:** Frontal sections of Atg7-deficient (Atg7<sup>flx/flx</sup>;Nes) (**A, C, E, G**) and its littermate control (Atg7<sup>flx/flx</sup>) (**B, D, F, H**) mouse brains 7 days after H/I injury. H&E (**A–D**) and NeuN (**E–H**) staining. **I:** Evaluation of the area loss in the ipsilateral hippocampus of Atg7-deficient ( $n = 11$ ) and littermate control ( $n = 12$ ) mouse brains 7 days after H/I injury. The mean value of the area loss in the ipsilateral hippocampus was significantly lower in Atg7-deficient mice (14.0) than in their littermate control mice (48.8).  $P < 0.0001$  (Mann-Whitney  $U$ -test) for the comparison of mean values between the two groups. Scale bars: 1000  $\mu$ m (**A, B, E, F**), 200  $\mu$ m (**C, D, G, H**).

of pyramidal neuron death in the hippocampus after H/I injury, we further analyzed the degree of damage in the neurons of the hippocampal pyramidal layers in Atg7-deficient and control littermate mouse brains 7 days after H/I injury. In fact, because shrunken or dying neurons with pyknotic nuclei were eliminated and the number of NeuN-positive surviving neurons was much reduced in the pyramidal layers of the control Atg7<sup>flx/flx</sup> mouse hippocampus 7 days after H/I injury, the pyramidal layers of the ipsilateral hippocampus were significantly diminished in area, compared to the contralateral hippocampus (Figure 7, B, D, F, and H). In Atg7-deficient mice, pyramidal neurons appeared intact in the hippocampus 7 days after H/I injury (Figure 7, A, C, E, and G). As far as we intensively measured the areas of the ipsi- and contralateral hippocampi 7 days after H/I injury, the area loss in the ipsilateral hippocampus that was expressed as a percentage of the contralateral hippocampal area was significantly much lower in the Atg7-deficient mice (14.0%) than in the littermate control mice (48.8%,  $P < 0.0001$ ) (Figure 7I). These data indicate that the prevention of hippocampal pyramidal neuron death after H/I injury by Atg7 deficiency in CNS tissue is sustained at least until 7 days after H/I injury.

#### Pathological Alterations Are Not Detected in the Hippocampal Pyramidal Neurons of Atg7-Deficient Neonatal Hippocampus after H/I Injury

Because H/I induced-pyramidal neuron death in the neonatal hippocampus was primarily prevented by Atg7 deficiency, we next examined whether Atg7 deficiency prevents caspase-independent neuron death only or both caspase-dependent and -independent neuron death. Immunohistochemical observations revealed that only very rare TUNEL-positive neurons were co-stained for cleaved caspase-3 in the pyramidal layers of Atg7-deficient hippocampus 24 hours after H/I injury (Figure 8, A and B), whereas abundant TUNEL-positive pyramidal neurons, some of which were co-stained for cleaved caspase-3, appeared in the control littermate hippocampus at the corresponding time point (Figure 8, C and D). By electron microscopy, the neuronal architecture in the pyramidal layers of the hippocampus appeared intact in Atg7-deficient mice 24 hours after H/I injury (Figure 8E). By Western blotting, the active forms of caspases-3 and -7 were not detected in the hippocampus lacking Atg7 after H/I injury, although cleaved caspase-3 was detected in the

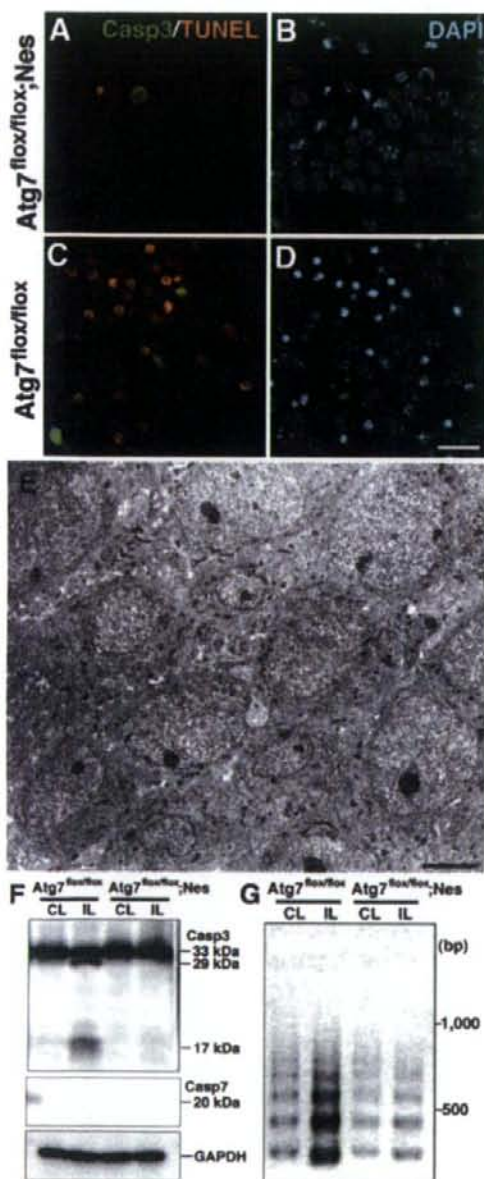


**Figure 8.** The apoptotic pathway is inhibited in the neonatal hippocampus after H/I injury by the Atg7 deficiency. **A–D:** Triple staining for cleaved caspase-3 (Casp3) (**A, C**), TUNEL (**A, C**), and DAPI (**B, D**) in the ipsilateral hippocampi of Atg7-deficient (*Atg7<sup>flox/flox</sup>; Nes*) (**A, B**) and control littermate (*Atg7<sup>flox/flox</sup>*) (**C, D**) mouse brains 24 hours after H/I injury. **E:** The neuronal cell architecture as well as morphological features of the neurons appeared intact in the hippocampal pyramidal layer of an Atg7-deficient mouse brain 24 hours after H/I injury. **F:** Western blotting of caspases-3 and -7 in the ipsilateral (IL) and contralateral hippocampi of littermate control (*Atg7<sup>flox/flox</sup>*) and Atg7-deficient (*Atg7<sup>flox/flox</sup>; Nes*) mouse brains 8 hours after H/I injury. Cleaved caspase-3, but not caspase-7, was detected only in the control IL hippocampus. GAPDH was used as a loading control. **G:** The DNA fragmentation in the ipsilateral (IL) and contralateral (CL) hippocampi from Atg7-deficient (*Atg7<sup>flox/flox</sup>; Nes*) and littermate (*Atg7<sup>flox/flox</sup>*) mouse brains 24 hours after H/I injury. Scale bars: 20  $\mu$ m (**A–D**); 5  $\mu$ m (**E**).

control littermate hippocampus 8 hours after H/I injury (Figure 8F). Moreover, as evidenced by LMP-PCR, the genomic DNA from hippocampi of control littermate mice after H/I injury was intensely fragmented into nucleosomes in the ipsilateral side and faintly in the contralateral side, whereas that from the hippocampus of Atg7-deficient mice was faintly fragmented into nucleosomes in both the ipsilateral and contralateral sides (Figure 8G). Because certain numbers of neurons in the mouse hippocampus undergo naturally occurring cell death at P8,<sup>47</sup> the DNA fragmentation observed in the contra- and ipsilateral hippocampi of Atg7-deficient mice might result from physiological neuron death in the hippocampus. Collectively, these results indicate that the Atg7 deficiency primarily prevented both caspase-3-dependent and caspase-3-independent neuron death in hippocampi from the neonatal mouse brains after H/I injury.

### Characteristic Features of H/I Injury-Induced Neuron Death in the Adult Hippocampus

We were not able to use specifically the CNS tissue of Atg7-deficient mice to examine the role of autophagy in adult H/I brain injury, because neurodegeneration, such as loss of pyramidal neurons in the hippocampus and

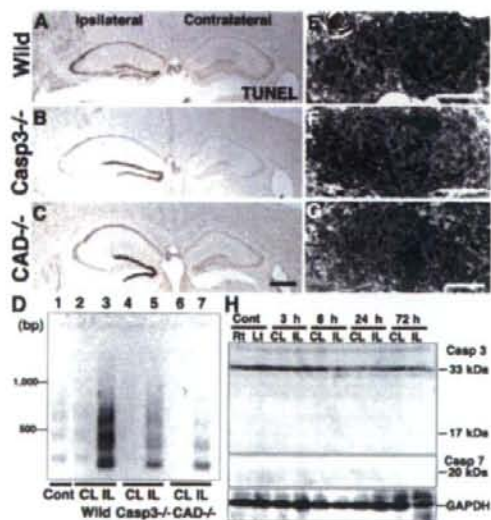


**Figure 9.** Pyramidal neuron death in the hippocampus of adult mouse brains after H/I injury. **A–C:** Frontal histological sections of wild-type (**A**) and caspase-3 deficient (*Casp3<sup>-/-</sup>*) (**B**) and CAD-deficient (*CAD<sup>-/-</sup>*) (**C**) brains including ipsilateral and contralateral hippocampi 24 hours after H/I injury. Staining with TUNEL. **D:** Genomic DNA fragmentation detected by LMP-PCR. Samples were obtained from the hippocampus of an untreated wild-type brain (Cont) (lane 1), and the contralateral (CL) and ipsilateral (IL) hippocampi of wild-type (lanes 2 and 3), caspase-3-deficient (lanes 4 and 5), and CAD-deficient (lanes 6 and 7) brains 24 hours after H/I injury. **E–G:** A nucleus with small patches of chromatin clumping was observed in the pyramidal neurons of not only wild-type (**E**) but also caspase-3-deficient (**F**) and CAD-deficient (**G**) mouse hippocampi 24 hours after H/I injury. **H:** The cleavage of caspases-3 and -7 in the contralateral (CL) and ipsilateral (IL) hippocampi of wild-type adult mouse brains at 3 hours, 8 hours, 24 hours, and 72 hours after H/I injury. Hippocampal tissues of the right (R) and left (L) sides from untreated adult mice were used as controls (Cont). Scale bars: 500  $\mu$ m (**C**); 2  $\mu$ m (**E–G**).

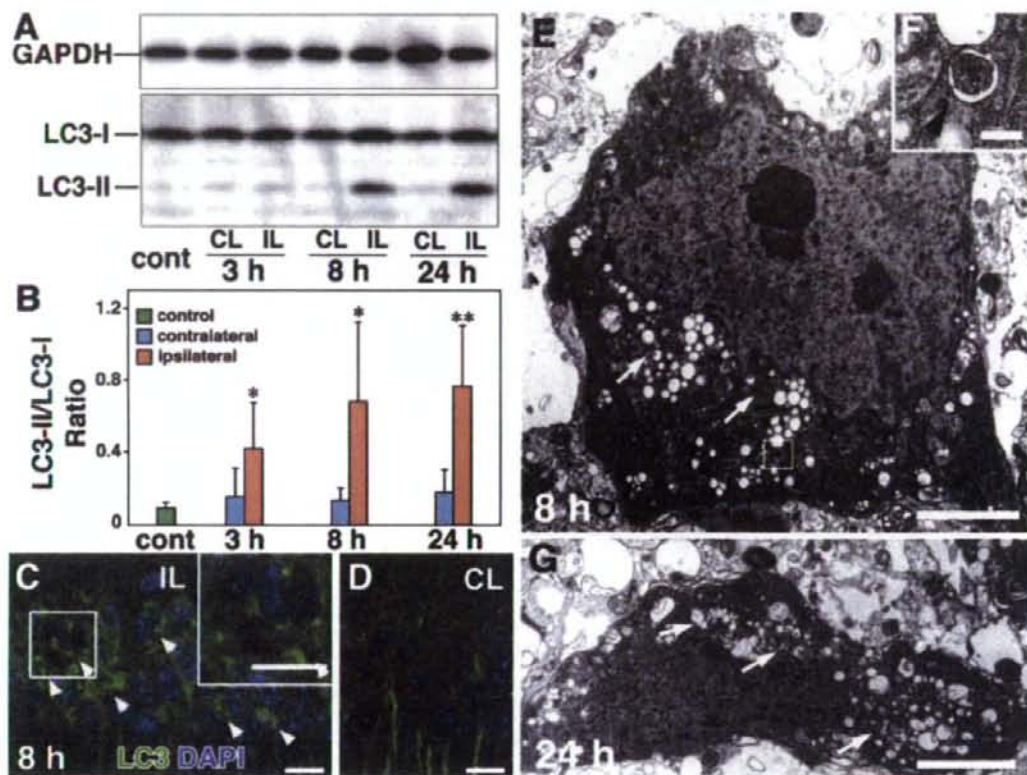


**Figure 10.** H/I injury induces autophagy in the hippocampus of wild-type and mutant adult mouse brains. **A:** Western blotting of LC3 in the untreated hippocampus (Cont) and the ipsilateral (IL) and contralateral (CL) hippocampi of adult mouse brains at 3, 8, and 24 hours after H/I injury. **B:** Quantification of **A**. The ratios of the amounts of LC3-II to LC3-I were calculated at each corresponding time. The final values represent the mean  $\pm$  SD for three animals. \* $P < 0.05$  and \*\* $P < 0.01$  (Student's *t*-test) for the comparison of the values between the ipsilateral and contralateral sides. **C and D:** Double staining of LC3 and DAPI in the ipsilateral (**C**) and contralateral (**D**) hippocampi of adult mouse brains 8 hours after H/I injury. **E-G:** Electron micrographs of a CA1 pyramidal neuron in the hippocampus of wild-type adult mouse brains 8 (**E, F**) and 24 (**G**) hours after H/I injury. Vacuolar structures with amorphous structures (**arrows**) are seen in **E** and **F**. A nascent autophagosome (**arrowhead**) (**boxed areas** in **E**). Scale bars: 10  $\mu$ m (**C, D**); 5  $\mu$ m (**E, G**); 0.5  $\mu$ m (**F**).

Purkinje cells in the cerebellum, manifests in the mutant mice from 3 weeks of age.<sup>36</sup> As shown in Figure 9H, H/I injury-dependent pyramidal neuron death did not require activation of caspases-3 and -7 in the adult wild-type hippocampus. Like neonatal mice, it is also evident that such pyramidal neuron death was not prevented in the hippocampus of caspase-3- or CAD-deficient mouse brains (Figure 9, A-C), whereas DNA laddering in the ipsilateral hippocampus was detected in each of these mouse brains (Figure 9D), indicating that the DNA fragmentation in H/I injury-induced adult pyramidal neuron death was mediated by an unknown DNase other than CAD. Moreover, alterations in nuclear chromatin were very similar to those in neonatal hippocampal neurons after H/I injury (Figure 9, E-G). Autophagic alterations were also detected in pyramidal neurons of the adult hippocampus after H/I injury; the ratio of the amounts of LC3-II to LC3-I was significantly higher in the ipsilateral side at each time point than in the contralateral side (Figure 10, A and B), whereas intense granular LC3-immunoreactivity was observed in hippocampal pyramidal

neurons with pyknotic nuclei after H/I injury (Figure 10, C and D; Supplemental Figure 1 see <http://ajp.amjpathol.org>). Notably autophagy seemed to be more pronounced in the ipsilateral hippocampus of adult mice than of neonates, judging from LC3-II/LC3-I ratio. By electron microscopy, pyramidal neurons that contained irregularly shaped nuclei with small patches of chromatin clumping often became shrunken and contained numerous vacuolar structures including autophagosomal and lysosomal structures (Figure 10, E-G), indicating that morphological features of these degenerating neurons resembled the features of type 2 neuron death.<sup>24</sup> These results suggest that autophagy also plays a pivotal role in the H/I-induced pyramidal neuron death in the adult hippocampus.

### Discussion

The present study demonstrated that 1) H/I injury-induced pyramidal neuron death in the neonatal hippocampus occurred in caspase 3-dependent and

caspase 3-independent manners. The caspase 3-independent neuron death in this model was accompanied by DNA ladder formation that was mediated by unknown DNase other than CAD. 2) H/I injury induced autophagy in neonatal hippocampal pyramidal neurons, whereas this pyramidal neuron death was prevented by Atg7 deficiency. 3) Pyramidal neuron death in the adult hippocampus after H/I injury was caspase-independent and accompanied by autophagosome formation.

### *Pyramidal Neuron Death in the Neonatal Hippocampus after H/I Injury*

Because numerous studies on neuron death after H/I brain injury using various animals have shown that the hippocampus is the most vulnerable to ischemic insult,<sup>9,13</sup> we examined how pyramidal neurons in the neonatal and adult hippocampi die after H/I injury. As shown in the Results section, nuclei of most pyramidal neurons in the hippocampus became pyknotic within 24 hours after H/I injury, indicating that the dying neurons were distinct from necrosis. It has been shown that caspase-3 may mediate ischemic neuron death in the rodent hippocampus.<sup>10,13,53</sup> In fact, we confirmed that 35% of total hippocampal pyramidal neurons underwent neuron death in a caspase-dependent manner. The ratio of neurons that died in a caspase-dependent manner is consistent with previous data shown by the use of a caspase-3 inhibitor<sup>44</sup> and Bcl-xL-overexpressing mice.<sup>14</sup> Although H/I injury-induced pyramidal neuron death in the neonatal hippocampus was in part caspase-dependent,<sup>10,13</sup> the genetic ablation of caspase-3 did not prevent H/I injury-induced pyramidal neuron death.<sup>44</sup> It has been shown that caspase-7, which is structurally and functionally similar to caspase-3, compensates for the lack of caspase-3.<sup>48,50</sup> In fact, in our H/I injury model using caspase-3-deficient mice, caspase-7 was activated in pyramidal neurons that underwent programmed cell death in the contralateral hippocampus at P8 (Figure 3A) and also weakly, but distinctly, in the pyramidal neurons of the ipsilateral hippocampus after H/I injury (Figure 3, E and F). Therefore, it seems likely that CAD in caspase-3-deficient mouse brains after H/I injury was activated by caspase-7 that was up-regulated in a compensatory way, resulting in DNA laddering.<sup>50</sup>

As shown in the present results, it is well known that a great number of pyramidal neurons in the neonatal hippocampus after H/I injury die in a caspase-independent manner.<sup>10</sup> To verify the involvement of this caspase-independent pathway in H/I injury-induced pyramidal neuron death in addition to the caspase-dependent pathway, neonatal CAD-deficient mice were subjected to H/I brain injury. Like caspase-3-deficient mice, H/I injury-induced pyramidal neuron death in the neonatal hippocampus was not prevented by CAD deficiency. It is very interesting that even in CAD-deficient mice, pyramidal neuron death in the hippocampus after H/I injury that was caspase-independent was accompanied by genomic DNA laddering, indicating that this DNA fragmentation was mediated by an unknown DNase other than CAD.

Collectively, H/I injury-induced pyramidal neuron death in the neonatal hippocampus was mediated by both caspase-dependent and -independent pathways.

### *Involvement of Autophagy in Neonatal Pyramidal Neuron Death after H/I Injury*

This is the first report that we are aware of providing direct evidence for autophagy-induced neuron death after neonatal mouse H/I brain injury, using mice that cannot execute autophagy specifically in CNS tissue.<sup>36</sup> As stated above, we demonstrated that pyramidal neuron death in the neonatal hippocampus after H/I injury was executed in both caspase-dependent and -independent manners, as has been shown previously.<sup>10,44</sup> Surprisingly, such caspase-dependent neuron death after H/I injury, along with caspase-independent neuron death, was prevented by selective CNS Atg7 deficiency. It has also been shown that autophagy participates in the initiation of apoptotic cell death such as photoreceptor cells exposed to oxidative stress and cerebellar granule cells after deprivation of serum and potassium.<sup>23,54</sup> As has been noted,<sup>30</sup> if autophagy would act as a survival factor in response to various stresses, hippocampal pyramidal neurons deficient in Atg7 would not be resistant to H/I injury. It is therefore important to reveal the molecular mechanism of how autophagy is involved in the activation of caspase cascade in H/I injury-induced pyramidal neuron death. These lines of evidence suggest that once H/I injury induces autophagy in pyramidal neurons of the neonatal hippocampus, autophagy may further activate two effectors, caspase-dependent (apoptotic) and -independent pathways of neuron death.

It has been shown that specific inhibitors of caspases attenuate H/I-induced pyramidal neuron death in the neonatal hippocampus.<sup>44,53</sup> Because there were caspase-dependent and -independent pathways of hippocampal pyramidal neuron death after neonatal brain H/I injury, the suppressive effects of these chemical agents and genetic manipulation such as Bcl-xL<sup>14</sup> would be limited to some extent. Thus far, chemical and genetically manipulated suppressors of autophagy that are available for therapeutic use have not been generated. Therefore, like caspase inhibitors, the development of chemical tools that prevent autophagic neuron death by specifically blocking each step of autophagy<sup>55</sup> may be important, because our data strongly suggest that autophagy regulates H/I-induced pyramidal neuron death in the neonatal hippocampus.

### *H/I Injury-Induced Pyramidal Neuron Death in the Adult Hippocampus Is Prevented by Neither Caspase-3 Nor CAD Deficiency*

The present data using caspase-3- or CAD-deficient mice also provide direct evidence that H/I injury-induced pyramidal neuron death in the adult hippocampus does not require the activation of caspase-3 and CAD. Such neuron death in the adult hippocampus was accompa-

nied by pyknosis and genomic DNA fragmentation into oligonucleosomes, indicating that pyramidal neuron death in the adult hippocampus after H/I injury is caspase-3-independent and distinct from necrosis. The present study could not examine the role of autophagy in adult H/I brain injury, because *Atg7<sup>loxP/loxP</sup>*; *nestin-Cre* mice manifested neurodegenerative signs such as loss of pyramidal neurons in the hippocampus and Purkinje cells in the cerebellum from 3 weeks of age.<sup>36</sup> Nevertheless, our current data showing that morphological features of degenerating neurons in the adult hippocampus after H/I injury resembled the features of type 2 neuron death,<sup>24</sup> suggest that autophagy is also involved in the execution of H/I injury-induced neuron death in the adult hippocampus. Thus, therapeutic strategies to inhibit autophagy-induced neuron death may prove beneficial in the treatment of both pediatric and adult H/I brain injury.

Collectively, at present, it remains unknown how the genetic ablation of *Atg7* specifically in the CNS prevents H/I injury-induced pyramidal neuron death in the neonatal hippocampus. It is well known that autophagy is essential for the maintenance of cellular metabolism and is induced in response to various stresses such as starvation, thus preventing cells from dying.<sup>18</sup> It is therefore very important to understand the mechanism of how pyramidal neurons regulate the two opposite downstream effects of autophagy, survival and death, after H/I insult.

### Acknowledgments

We thank K. Ikeue, K. Ohta, A. Koseki, and K. Isahara for technical assistance.

### References

1. du Plessis AJ, Volpe JJ: Perinatal brain injury in the preterm and term newborn. *Curr Opin Neurol* 2002, 15:151-157
2. Hamrick SE, Ferriero DM: The injury response in the term newborn brain: can we neuroprotect? *Curr Opin Neurol* 2003, 16:147-154
3. Ashwal S, Pearce WJ: Animal models of neonatal stroke. *Curr Opin Pediatr* 2001, 13:506-516
4. Ferriero DM: Neonatal brain injury. *N Engl J Med* 2004, 351:1985-1995
5. Hagberg H, Bona E, Gilland E, Puka-Sundvall M: Hypoxia-ischaemia model in the 7-day-old rat: possibilities and shortcomings. *Acta Paediatr Suppl* 1997, 422:85-88
6. Levine S: Anoxic-ischemic encephalopathy in rats. *Am J Pathol* 1960, 36:1-17
7. Sheldon RA, Hall JJ, Noble LJ, Ferriero DM: Delayed cell death in neonatal mouse hippocampus from hypoxia-ischemia is neither apoptotic nor necrotic. *Neurosci Lett* 2001, 304:165-168
8. Blomgren K, Leist M, Groc L: Pathological apoptosis in the developing brain. *Apoptosis* 2007, 12:993-1010
9. Sheldon RA, Sedik C, Ferriero DM: Strain-related brain injury in neonatal mice subjected to hypoxia-ischemia. *Brain Res* 1998, 810:114-122
10. Zhu C, Wang X, Xu F, Bahr BA, Shibata M, Uchiyama Y, Hagberg H, Blomgren K: The influence of age on apoptotic and other mechanisms of cell death after cerebral hypoxia-ischemia. *Cell Death Differ* 2005, 12:162-176
11. Calvert JW, Zhang JH: Pathophysiology of an hypoxic-ischemic insult during the perinatal period. *Neurol Res* 2005, 27:246-260
12. Gibson ME, Han BH, Choi J, Knudson CM, Korsmeyer SJ, Parsadanian M,

- Holtzman DM: BAX contributes to apoptotic-like death following neonatal hypoxia-ischemia: evidence for distinct apoptosis pathways. *Mol Med* 2001, 7:644-655
13. Ness JM, Harvey CA, Strasser A, Bouillet P, Klocke BJ, Roth KA: Selective involvement of BH3-only Bcl-2 family members Bim and Bad in neonatal hypoxia-ischemia. *Brain Res* 2006, 1099:150-159
14. Parsadanian AS, Cheng Y, Keller-Peck CR, Holtzman DM, Snider WD: Bcl-xL is an antiapoptotic regulator for postnatal CNS neurons. *J Neurosci* 1998, 18:1009-1019
15. Perlman JM: Intervention strategies for neonatal hypoxic-ischemic cerebral injury. *Clin Ther* 2006, 28:1353-1365
16. Komatsu M, Waguri S, Ueno T, Iwata J, Murata S, Tanida I, Ezaki J, Mizushima N, Ohsumi Y, Uchiyama Y, Kominami E, Tanaka K, Chiba T: Impairment of starvation-induced and constitutive autophagy in *Atg7*-deficient mice. *J Cell Biol* 2005, 169:425-434
17. Kuma A, Hatano M, Matsui M, Yamamoto A, Nakaya H, Yoshimori T, Ohsumi Y, Tokuhisa T, Mizushima N: The role of autophagy during the early neonatal starvation period. *Nature* 2004, 432:1032-1036
18. Shintani T, Klionsky DJ: Autophagy in health and disease: a double-edged sword. *Science* 2004, 306:990-995
19. Zhu JH, Horbinski C, Guo F, Watkins S, Uchiyama Y, Chu CT: Regulation of autophagy by extracellular signal-regulated protein kinases during 1-methyl-4-phenylpyridinium-induced cell death. *Am J Pathol* 2007, 170:75-86
20. Nixon RA: Autophagy in neurodegenerative disease: friend, foe or turncoat? *Trends Neurosci* 2006, 29:528-535
21. Koike M, Shibata M, Waguri S, Yoshimura K, Tanida I, Kominami E, Gotow T, Peters C, von Figura K, Mizushima N, Saftig P, Uchiyama Y: Participation of autophagy in storage of lysosomes in neurons from mouse models of neuronal ceroid-lipofuscinoses (Batten disease). *Am J Pathol* 2005, 167:1713-1728
22. Chu CT: Autophagic stress in neuronal injury and disease. *J Neuro-pathol Exp Neurol* 2006, 65:423-432
23. Canu N, Tuli R, Seralino AL, Amadoro G, Ciotti MT, Calissano P: Role of the autophagic-lysosomal system on low potassium-induced apoptosis in cultured cerebellar granule cells. *J Neurochem* 2005, 92:1228-1242
24. Clarke PG: Developmental cell death: morphological diversity and multiple mechanisms. *Anat Embryol (Berl)* 1990, 181:195-213
25. Ohsawa Y, Isahara K, Kanamori S, Shibata M, Kametaka S, Gotow T, Watanabe T, Kominami E, Uchiyama Y: An ultrastructural and immunohistochemical study of PC12 cells during apoptosis induced by serum deprivation with special reference to autophagy and lysosomal cathepsins. *Arch Histol Cytol* 1998, 61:395-403
26. Uchiyama Y: Autophagic cell death and its execution by lysosomal cathepsins. *Arch Histol Cytol* 2001, 64:233-246
27. Nitatori T, Sato N, Waguri S, Karasawa Y, Araki H, Shibana I, Kominami E, Uchiyama Y: Delayed neuronal death in the CA1 pyramidal cell layer of the gerbil hippocampus following transient ischemia is apoptosis. *J Neurosci* 1995, 15:1001-1011
28. Zhu C, Xu F, Wang X, Shibata M, Uchiyama Y, Blomgren K, Hagberg H: Different apoptotic mechanisms are activated in male and female brains after neonatal hypoxia-ischaemia. *J Neurochem* 2006, 96:1016-1027
29. Kabeya Y, Mizushima N, Ueno T, Yamamoto A, Kirisako T, Noda T, Kominami E, Ohsumi Y, Yoshimori T: LC3, a mammalian homologue of yeast Apg8p, is localized in autophagosome membranes after processing. *EMBO J* 2000, 19:5720-5728
30. Levine B, Yuan J: Autophagy in cell death: an innocent convict? *J Clin Invest* 2005, 115:2679-2688
31. Rice JE III, Vannucci RC, Brierley JB: The influence of immaturity on hypoxic-ischemic brain damage in the rat. *Ann Neurol* 1981, 9:131-141
32. Tronche F, Kellendonk C, Kretz O, Gass P, Anlag K, Orban PC, Bock R, Klein R, Schutz G: Disruption of the glucocorticoid receptor gene in the nervous system results in reduced anxiety. *Nat Genet* 1999, 23:99-103
33. Kawane K, Fukuyama H, Yoshida H, Nagase H, Ohsawa Y, Uchiyama Y, Okada K, Iida T, Nagata S: Impaired thymic development in mouse embryos deficient in apoptotic DNA degradation. *Nat Immunol* 2003, 4:138-144
34. Kuida K, Zheng TS, Na S, Kuan C, Yang D, Karasuyama H, Rakic P, Flavell RA: Decreased apoptosis in the brain and premature lethality in CPP32-deficient mice. *Nature* 1996, 384:368-372

35. Leonard JR, Klocke BJ, D'Sa C, Flavell RA, Roth KA: Strain-dependent neurodevelopmental abnormalities in caspase-3-deficient mice. *J Neuropathol Exp Neurol* 2002, 61:673-677
36. Komatsu M, Waguri S, Chiba T, Murata S, Iwata J, Tanida I, Ueno T, Koike M, Uchiyama Y, Kominami E, Tanaka K: Loss of autophagy in the central nervous system causes neurodegeneration in mice. *Nature* 2006, 441:880-884
37. Lu Z, Dono K, Gotoh K, Shibata M, Koike M, Marubashi S, Miyamoto A, Takeda Y, Nagano H, Umeshita K, Uchiyama Y, Monden M: Participation of autophagy in the degeneration process of rat hepatocytes after transplantation following prolonged cold preservation. *Arch Histol Cytol* 2005, 68:71-80
38. Tanida I, Mizushima N, Kiyooka M, Ohsumi M, Ueno T, Ohsumi Y, Kominami E: Apg7p/Cvt2p: a novel protein-activating enzyme essential for autophagy. *Mol Biol Cell* 1999, 10:1367-1379
39. Koike M, Nakanishi H, Saftig P, Ezaki J, Isahara K, Ohsawa Y, Schulz-Schaeffer W, Watanabe T, Waguri S, Kametaka S, Shibata M, Yamamoto K, Kominami E, Peters C, von Figura K, Uchiyama Y: Cathepsin D deficiency induces lysosomal storage with ceroid lipofuscin in mouse CNS neurons. *J Neurosci* 2000, 20:6898-6906
40. Koike M, Shibata M, Ohsawa Y, Nakanishi H, Koga T, Kametaka S, Waguri S, Momoi T, Kominami E, Peters C, Figura K, Saftig P, Uchiyama Y: Involvement of two different cell death pathways in retinal atrophy of cathepsin D-deficient mice. *Mol Cell Neurosci* 2003, 22:146-161
41. Gavrieli Y, Sherman Y, Ben-Sasson SA: Identification of programmed cell death in situ via specific labeling of nuclear DNA fragmentation. *J Cell Biol* 1992, 119:493-501
42. Paxinos G, Franklin BJK: *The Mouse Brain in Stereotaxic Coordinates*. San Diego, Academic Press, 2001
43. Staley K, Blaschke AJ, Chun J: Apoptotic DNA fragmentation is detected by a semi-quantitative ligation-mediated PCR of blunt DNA ends. *Cell Death Differ* 1997, 4:66-75
44. West T, Atzeva M, Holtzman DM: Caspase-3 deficiency during development increases vulnerability to hypoxic-ischemic injury through caspase-3-independent pathways. *Neurobiol Dis* 2006, 22:523-537
45. Towbin H, Staehelin T, Gordon J: Electrophoretic transfer of proteins from polyacrylamide gels to nitrocellulose sheets: procedure and some applications. *Proc Natl Acad Sci USA* 1979, 76:4350-4354
46. Klaunig JE, Goldblatt PJ, Hinton DE, Lipsky MM, Chacko J, Trump BF: Mouse liver cell culture. I. Hepatocyte isolation. *In Vitro* 1981, 17:913-925
47. Reznikov KY: Cell proliferation and cytogenesis in the mouse hippocampus. *Adv Anat Embryol Cell Biol* 1991, 122:1-74
48. Lakhani SA, Masud A, Kuida K, Porter GA Jr, Booth CJ, Mehal WZ, Inayat I, Flavell RA: Caspases 3 and 7: key mediators of mitochondrial events of apoptosis. *Science* 2006, 311:847-851
49. Enari M, Sakahira H, Yokoyama H, Okawa K, Iwamatsu A, Nagata S: A caspase-activated DNase that degrades DNA during apoptosis, and its inhibitor ICAD. *Nature* 1998, 391:43-50
50. Houde C, Banks KG, Coulombe N, Rasper D, Grimm E, Roy S, Simpson EM, Nicholson DW: Caspase-7 expanded function and intrinsic expression level underlies strain-specific brain phenotype of caspase-3-null mice. *J Neurosci* 2004, 24:9977-9984
51. Yu L, Alva A, Su H, Dutt P, Freundt E, Welsh S, Baehrecke EH, Lenardo MJ: Regulation of an ATG7-beclin 1 program of autophagic cell death by caspase-8. *Science* 2004, 304:1500-1502
52. Tanida I, Tanida-Miyake E, Komatsu M, Ueno T, Kominami E: Human Apg3p/Aut1p homologue is an authentic E2 enzyme for multiple substrates. GATE-16, GABARAP, and MAP-LC3, and facilitates the conjugation of hApg12p to hApg5p. *J Biol Chem* 2002, 277:13739-13744
53. Cheng Y, Deshmukh M, D'Costa A, Demaro JA, Gidday JM, Shah A, Sun Y, Jacquin MF, Johnson EM, Holtzman DM: Caspase inhibitor affords neuroprotection with delayed administration in a rat model of neonatal hypoxic-ischemic brain injury. *J Clin Invest* 1998, 101:1992-1999
54. Kunchithapautham K, Rohrer B: Apoptosis and autophagy in photoreceptors exposed to oxidative stress. *Autophagy* 2007, 3:433-441
55. Rubinsztein DC, Gestwicki JE, Murphy LO, Klionsky DJ: Potential therapeutic applications of autophagy. *Nat Rev Drug Discov* 2007, 6:304-312



## A Neural-specific F-box Protein Fbs1 Functions as a Chaperone Suppressing Glycoprotein Aggregation\*

Received for publication, December 5, 2006. Published, JBC Papers in Press, January 10, 2007, DOI 10.1074/jbc.M611168200

Yukiko Yoshida<sup>§1</sup>, Arisa Murakami<sup>§5</sup>, Kazuhiro Iwai<sup>§6</sup>, and Keiji Tanaka<sup>‡</sup>

From the <sup>§</sup>Tokyo Metropolitan Institute of Medical Science, 3-18-22 Honkomagome, Bunkyo-ku, Tokyo 113-8613, <sup>¶</sup>CREST, Japan Science and Technology Corporation (JST), Saitama 332-0012, and the <sup>‡</sup>Department of Molecular Cell Biology, Graduate School of Medicine, Osaka City University, 1-4-3 Asahi-cyo, Abeno-ku, Osaka 545-8585, Japan

Fbs1 is an F-box protein present abundantly in the nervous system. Similar to the ubiquitously expressed Fbs2, Fbs1 recognizes N-glycans at the innermost position as a signal for unfolded glycoproteins, probably in the endoplasmic reticulum-associated degradation pathway. Here, we show that the *in vivo* majority of Fbs1 is present as Fbs1-Skp1 heterodimers or Fbs1 monomers but not SCF<sup>Fbs1</sup> complex. The inefficient SCF complex formation of Fbs1 and the restricted presence of SCF<sup>Fbs1</sup> bound on the endoplasmic reticulum membrane were due to the short linker sequence between the F-box domain and the sugar-binding domain. *In vitro*, Fbs1 prevented the aggregation of the glycoprotein through the N-terminal unique sequence of Fbs1. Our results suggest that Fbs1 assists clearance of aberrant glycoproteins in neuronal cells by suppressing aggregates formation, independent of ubiquitin ligase activity, and thus functions as a unique chaperone for those proteins.

The SCF (Skp1/Cul1/E-box protein) complex, the largest known class of sophisticated E3<sup>2</sup> ubiquitin ligases, consists of common components, Skp1, Cul1, and Roc1/Rbx1, as well as variable components known as F-box proteins that bind the substrates (1, 2). In this complex, the scaffold protein Cul1 (alias cullin1) interacts at the N terminus with the adaptor subunit Skp1 and at the C terminus with the RING-finger protein Roc1/Rbx1 that recruits a specific ubiquitin-activating enzyme (E2) for ubiquitylation. F-box proteins, interacting with Skp1 through the ~40 amino acid F-box motif, play an indispensable role in the selection of target proteins for degradation because each distinct F-box protein usually binds a protein substrate(s) with a degree of selectivity for ubiquitylation through C-terminal protein-protein interaction domains (3). The human genome contains 69 genes for F-box proteins and a large number of F-box proteins function in the specific ubiquitylation of a wide range of substrates. The F-box proteins are divided into three classes according to the type of substrate-binding domains. The two classes of binding domains are WD40

repeats and leucine-rich repeats, which are named Fbw (or FBXW) and Fbl (or FBXL) families, respectively (4). The third class of F-box proteins is the Fbx (or FBXO) family that does not contain any of these domains.

It has been reported that a subfamily under the Fbx family consists of at least five homologous F-box proteins containing a conserved FBA motif (5, 6). Among them, Fbs1/Fbx2/NFB42/Fbg1 and Fbs2/Fbx6b/Fbg2 can bind to proteins with high mannose oligosaccharides modification that occurs in the endoplasmic reticulum (ER) (7). Experiments using a fully reconstituted system showed that both Fbs1 and Fbs2 can form SCF-type ubiquitin ligase complexes specific for N-linked glycoproteins (7, 8). Overexpression of the Fbs1 or Fbs2 dominant-negative form or decrease of endogenous Fbs2 by small interfering RNA resulted in inhibition of degradation of endoplasmic reticulum-associated degradation (ERAD) substrates, suggesting the involvement of SCF<sup>Fbs1</sup> and SCF<sup>Fbs2</sup> in the ERAD pathway. Interestingly, x-ray crystallographic and NMR studies of the substrate-binding domain of Fbs1 have revealed that Fbs1 interacts with the innermost chitobiose in N-glycans of glycoproteins by a small hydrophobic pocket located at the top of the  $\beta$ -sandwich, indicating that both Fbs1 and Fbs2 efficiently recognize the inner chitobiose structure in Man<sub>3-9</sub>GlcNAc<sub>2</sub> glycans (9). Indeed, the introduction of point mutation into the residues in the pocket impaired the binding activity toward its glycoprotein substrates. In general, the internal chitobiose structure of N-glycans in many native glycoproteins is not accessible by macromolecules. Fbs1 interacted with denatured glycoproteins more efficiently than native proteins, indicating that the innermost position of N-glycans becomes exposed upon protein denaturation and used as a signal of unfolded glycoproteins to be recognized by Fbs1 (10).

Of the Fbs family proteins, whereas Fbs2 is distributed ubiquitously in a variety of cells and tissues, Fbs1 is expressed only in neurons (7). In considering the involvement of these F-box proteins in the ERAD pathway in general, the restricted expression of Fbs1 in neurons remains a mystery. In this study, we found that the major population of Fbs1 protein did not form the SCF<sup>Fbs1</sup> complex in cells although Fbs1 is known to act as a compartment of SCF-type ubiquitin ligase (8). Moreover, the results showed that the sequence of the intervening segment between the F-box domain and the substrate-binding domain of the Fbs1 hampered the assembly of the SCF<sup>Fbs1</sup> complex in the cytosol without affecting the association with Skp1. The Skp1-Fbs1 heterodimers as well as SCF<sup>Fbs1</sup> complex effectively prevented the aggregation of the glycoprotein *in vitro*, and this

\* This work was supported by grants from the Ministry of Education Science and Culture of Japan (to Y. Y. and K. T.). The costs of publication of this article were defrayed in part by the payment of page charges. This article must therefore be hereby marked "advertisement" in accordance with 18 U.S.C. Section 1734 solely to indicate this fact.

<sup>1</sup> To whom correspondence should be addressed. Tel: 81-3-3823-2105; Fax: 81-3-3823-2965; E-mail: yyosida@rinshoken.or.jp.

<sup>2</sup> The abbreviations used are: E3, ubiquitin ligase; ER, endoplasmic reticulum; ERAD, ER-associated degradation; TBS, Tris-buffered saline; RNaseB, ribonuclease B; HA, hemagglutinin.

## In Vitro Chaperone Functions of Skp1-Fbs1

activity was dependent on the presence of the N-terminal domain and the substrate-binding domain of Fbs1. Our data thus imply that Skp1 and Fbs1 may function in both SCF and non-SCF complexes.

### EXPERIMENTAL PROCEDURES

**Affinity Purification and Immunoprecipitation of Brain Lysate**—The preparation of lysates from mouse brains and purification of Fbs1 by using a ribonuclease B (RNaseB) column were performed as described previously (10). For immunoprecipitation, we used polyclonal antibody to Fbs1 as described previously (11). For immunoblotting, we used rabbit polyclonal antibodies against Fbs1, Cull1 (Zymed Laboratories Inc., San Francisco, CA) and Skp1 (Santa Cruz Biotechnology, Santa Cruz, CA), and horseradish peroxidase-conjugated goat anti-rabbit IgG (Jackson ImmunoResearch Laboratories, West Grove, PA) for Fbs1 and Skp1 blots or horseradish peroxidase-conjugated goat anti-rabbit IgG light chain (Jackson ImmunoResearch Laboratories) for Cull1 blots. Lectin blotting was performed by using horseradish peroxidase-conjugated ConA (Seikagaku-kogyo, Japan) as described previously (11).

**Glycerol Gradient Analysis**—The fraction eluted with 0.1 M chitobiose from the RNaseB resin was prepared from 0.5 ml of lysates (14 mg/ml) from mouse brains. The eluate was dialyzed against TBS. The resultant fraction and a 1-mg lysate of brains were used for glycerol gradient analysis. Samples and molecular weight markers (Amersham Biosciences) were fractionated by 4–17% (v/v) linear glycerol density gradient centrifugation (22 h, 100,000 × g) as described previously (12).

**Cell Culture and Immunological Analysis**—PC12 cells were grown in RPMI medium 1640 (Invitrogen) supplemented with 10% horse serum and 5% fetal bovine serum. For neuronal differentiation, PC12 cells were treated with 10–20 ng/ml nerve growth factor (Invitrogen) on collagen-coated plates. 293T and HeLa cells were grown in Dulbecco's modified Eagle's medium (Sigma) supplemented with 10% fetal bovine serum and were transfected as described previously (8). FLAG-tagged Fbs1 mutant vectors consisting of Fbs1 and Fbs2 fragments were generated by PCR, and those sequences were verified. Whole cell lysates were prepared with 20 mM Tris-HCl (pH 7.5), 150 mM NaCl (TBS) containing 0.5% Nonidet P-40. The supernatant and precipitate fractions were prepared by ultracentrifugation of the supernatant that was prepared by centrifugation of freezing-and-thawing cell lysates in TBS at 8,000 × g for 20 min and at 100,000 × g for 60 min. The precipitate fraction was solubilized with Triton X-100. Each immunoprecipitation analysis was performed for whole cell lysates or subcellular fraction of cells by using the same amount of proteins. Monoclonal antibodies to calnexin and rhodopsin were purchased from BD Transduction Laboratories and Affinity Bioreagents (Golden, CO), respectively. Antibodies to FLAG, HA, and fetuin have been described previously (8).

**Pulse-chase Analysis**—The expression plasmid for P23H rhodopsin was kindly provided by M. E. Cheetham (University College London). Pulse-chase experiments were performed as described previously (7). Briefly, 293T cells were transfected with 1 μg of P23H rhodopsin expression plasmid and 1 μg of FLAG-tagged Fbs1 derivatives or pcDNA3-FLAG plasmid.

Twenty-four hours after transfection, the cells were starved for 30 min and labeled for 1 h with 150 μCi of Pro-Mix L-<sup>35</sup>S *in vitro* cell labeling mix (Amersham Biosciences) per milliliter. After washing, the cells were chased with complete Dulbecco's modified Eagle's medium supplemented with fetal bovine serum in the presence or in the absence of 50 μg/ml MG132 (Peptide Institute, Tokyo, Japan) for the indicated time intervals. After the harvested cells were lysed by TBS containing 0.1% SDS and 1% Nonidet P-40, immunoprecipitation was performed with anti-rhodopsin and FLAG antibodies.

**Preparation of Recombinant Proteins and *In Vitro* Ubiquitylation Assay**—The His-tagged Fbs1 ΔF, Fbs1 ΔP baculovirus were produced by Bac-to-Bac baculovirus expression system (Invitrogen). The SCF<sup>Fbs1</sup>, Skp1-Fbs1 dimers, Fbs1 Fbs1 ΔF, Fbs1 ΔP, Skp1-ΔP dimers, and Fbs1 ΔN were obtained by baculovirus-infected HighFive cells as described previously (10). These proteins were purified by affinity chromatography using RNaseB-immobilized beads as a ligand and chitobiose as an eluent, and the eluates were dialyzed to 1,000 volumes of TBS three times. *In vitro* ubiquitylation assays were performed as described previously (10).

**Aggregation Assay**—Jack bean α-mannosidase (Sigma) was desalted using a NAP-25 gel filtration column (Amersham Biosciences) equilibrated in 10 mM Tris-HCl (pH 8.0). The desalted protein was lyophilized and redissolved at 21.7 μM in 0.1 M Tris-HCl (pH 8.0) and 6 M GdnHCl as described previously (13). After denaturation for 60 min at room temperature, samples were diluted to 0.3 μM in 1 ml of TBS containing various concentrations of bovine serum albumin or recombinant Fbs1 derivatives. Protein aggregation was monitored at 25 °C over a period of 60 min by measuring absorbance at 360 nm.

### RESULTS

**Multiple States of Fbs1 in Brain**—Fbs1 has been found in the fraction eluted with di-N-acetyl-D-glucosamine (thereafter referred to as chitobiose) from GlcNAc-terminated fetuin of lysates prepared from mouse brain (8). Fbs1 and Skp1 proteins were detected in the eluted fraction with Coomassie Brilliant Blue staining, but we could not detect the apparent band of Cull1. However, the formation of the SCF<sup>Fbs1</sup> complex was confirmed not only by reciprocal immunoprecipitation experiments in 293T cells but also by reconstitution of baculovirally expressed recombinant SCF<sup>Fbs1</sup> proteins. To address these contradictory observations, we tested whether endogenous Fbs1 in the mouse brain forms the SCF complex by examining the interaction of Fbs1 with Cull1 (Fig. 1A). Fbs1 can be easily purified by affinity chromatography using RNaseB that contains a high mannose oligosaccharide as a ligand and chitobiose as an eluent (10). Since Fbs1 contains a single binding domain toward an N-glycan, it seems likely that the eluted Fbs1 protein or its complex from the RNaseB-immobilized resin is free from its substrates. Indeed, the glycoproteins modified with high mannose oligosaccharides were not included in the eluates by chitobiose (Fig. 1B). Although Skp1 was effectively co-immunoprecipitated with Fbs1 from the lysate of mouse brain, the amount of Skp1 that was eluted with Fbs1 from the RNaseB resin was small (Fig. 1A). Despite the difference in the quantities of Skp1 bound to Fbs1 in the fractions between eluates from

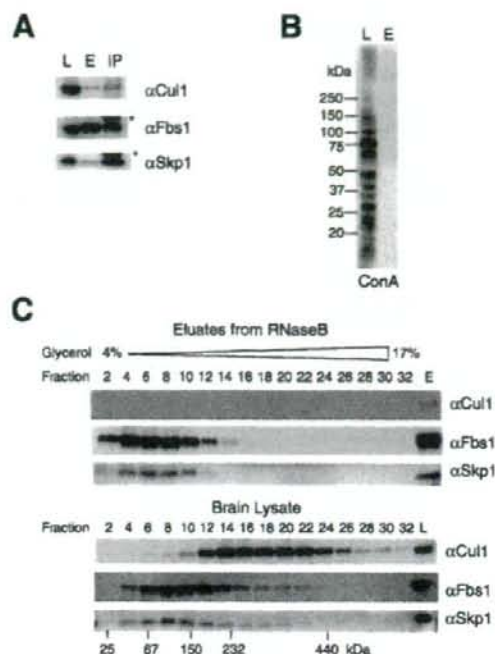


**FIGURE 1. States of Fbs1 in mouse brain.** A, 0.6 mg of lysate from adult mouse brain was subjected to RNaseB-immobilized affinity column and eluted with chitobiose (E) or subjected to immunoprecipitation with an antibody to Fbs1 (IP). Thirty  $\mu$ g of lysate (L), one-tenth of eluate, and immunoprecipitate were analyzed by immunoblotting with antibodies to Cul1, Fbs1, or Skp1. Asterisks show Ig heavy chain ( $\alpha$ Fbs1) and light chain ( $\alpha$ Skp1). B, ConA lectin blot for brain lysate (L) and the eluate from the RNaseB resin (E) against the same amounts of proteins described in A. C, adult mouse brain lysate (lower panel, 0.7 mg) and lysate eluted with chitobiose from RNaseB (upper panel, started from 7 mg of the lysate) were separated by 4–17% glycerol density gradient centrifugation. One-third of each fraction was analyzed by immunoblotting with antibodies to Cul1, Fbs1, and Skp1. Molecular size markers are indicated below.

the RNaseB resin and immunoprecipitation with an anti-Fbs1 antibody, almost the same and small quantities of Cul1 were detected in these fractions. These results suggest that major populations of substrate-free Fbs1 and substrate-binding Fbs1 are present as Fbs1 monomers and Fbs1-Skp1 dimers, respectively, and the binding of substrates to Fbs1 does not influence the weak SCF complex formation.

To examine the behavior of endogenous Fbs1 in more detail, eluates from the RNaseB resin and lysates from the mouse brain were separated by a 4–17% glycerol density gradient centrifugation (Fig. 1C). The distribution of Fbs1 (~42 kDa) in the chitobiose eluates corresponded to the position of Fbs1 monomers (fraction 4) and Skp1-Fbs1 dimers (~63 kDa) (fraction 6). Although Cul1 was not detected in any fractions, the peak of Skp1 in eluates from the RNaseB resin was in the position of the Skp1-Fbs1 dimer. On the other hand, Fbs1 protein in brain lysate was detected in a broad range of fractions mainly larger than Fbs1-Skp1 dimers, indicating that most Fbs1, if not all, is associated with various glycoprotein substrates; i.e. Fbs1-Skp1 dimers maintain the association with glycoproteins *in vivo*. Cul1 (~90 kDa) in brain lysate was distributed broadly in

higher density fractions, indicating its association with various other SCF-components.

**Minor Population of Fbs1 Forms SCF Complex on ER**—We next expressed FLAG-tagged F-box proteins alone or their combination with HA-tagged Skp1 in 293T cells and immunoprecipitated with anti-FLAG and anti-HA antibodies (Fig. 2A). The expression of HA-tagged Skp1 increased the amount of exogenous F-box proteins, suggesting that Skp1 stabilizes F-box proteins (lanes 1–8). Cul1 was co-immunoprecipitated with Fbs2 and Fbg3, which are highly homologous with Fbs1, or  $\beta$ TrCP1/Fbw1, one of the Fbw family members (lanes 11–16). The interaction between Cul1 and these F-box proteins increased upon co-expression of Skp1. However, unlike these F-box proteins, Fbs1 was almost undetectable in the immune complex with Cul1, regardless of the overexpression of exogenous Skp1 (lanes 9 and 10), although Fbs1 was co-immunoprecipitated with Skp1 as well as other F-box proteins (lanes 18, 20, 22, and 24 in the  $\alpha$ Flag panel). Moreover, the amount of Cul1 associated with exogenous Skp1 was lower in the presence of Fbs1 than in those of other F-box proteins, suggesting that expression of Fbs1 prevents forming other SCF complexes by dimerizing with Skp1 (lanes 18, 20, 22, and 24 in the  $\alpha$ Cul1 panel). These results suggest that Fbs1 can strongly bind Skp1 but is weak in forming the SCF<sup>Fbs1</sup> complex.

We have recently reported that Fbs1 is a cytosolic protein but that part of Fbs1 associates with the ER membrane through interaction with p97/VCP (valosin-containing protein) (11). We next examined whether the ER membrane-associated Fbs1 formed the SCF complex. Lysates of 293T and HeLa cells expressing FLAG-tagged Fbs1 were fractionated into the 100,000  $\times$  g supernatant and precipitate fractions excluding the 8,000  $\times$  g precipitate, and then Fbs1 was immunoprecipitated from these fractions by anti-FLAG antibody. As shown in Fig. 2B, Cul1 was co-immunoprecipitated with Fbs1 mainly from the precipitate (p) fraction (lanes 4 and 8). Although the association of Fbs1 with Skp1 occurred more effectively in the supernatant (s) fraction, the formation of the SCF complex, including Fbs1, was hardly detected in the supernatant fraction (lanes 3 and 7). Moreover, we examined whether endogenous Fbs1 formed the SCF complex in the precipitate fraction using nerve growth factor-treated PC12 cells, which endogenously express Fbs1 (14). As shown in Fig. 2C, part of Cul1 was co-immunoprecipitated with Fbs1 from the precipitate (p) fraction. These results indicate that the major population of endogenous Fbs1 is present as the Fbs1-Skp1 heterodimers or the Fbs1 monomers in the cytosol, and a minor population of Fbs1 forms the SCF complex bound on the ER membrane.

**Linker Sequence of Fbs1 Prevents SCF Complex Formation**—Although the SCF complex formation of Fbs1 was inefficient, Fbs2 formed the SCF complex effectively (Fig. 2A). To identify the region(s) of Fbs1 that impedes SCF complex formation, we examined the ability of various fusion proteins containing Fbs1 and Fbs2 fragments to form the complex and compared these findings with the full-length proteins in co-immunoprecipitation assay (Fig. 3A). Fbs1  $\Delta$ F was used as negative control that did not bind to Skp1 (Fig. 3B, lane 3). Fbs1 YW and Fbs1  $\Delta$ C, both of which are deficient in substrate binding, could not restore SCF complex formation, indicating that the interaction

## In Vitro Chaperone Functions of Skp1-Fbs1

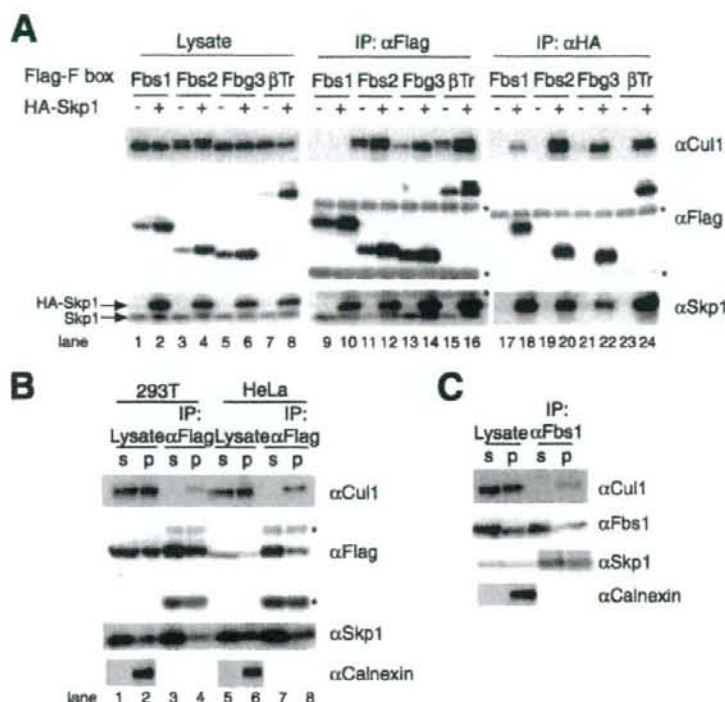


**FIGURE 2. Major population of Fbs1 forms non-SCF complex in vivo.** *A*, 293T cells were transfected with plasmids encoding various FLAG-tagged F-box proteins (Fbs1, Fbs2, Fbg3, and  $\beta$ TrCP1 ( $\beta$ Tr)) combination with empty HA plasmids (–) or plasmids encoding HA-tagged Skp1 (+). Whole cell lysates were subjected to immunoprecipitation (IP) with antibodies to FLAG and HA, and lysates (15  $\mu$ g each) and one half of the resulting precipitates were analyzed by immunoblotting with antibodies to Cull1, FLAG, and Skp1. Asterisks show Ig heavy and light chains. *B*, 293T and HeLa cells were transfected with FLAG-tagged Fbs1. Cell lysates were fractionated by ultracentrifugation, and FLAG-Fbs1 was immunoprecipitated with an antibody to FLAG from the same amount of proteins of 100,000  $\times$  g supernatant (s) and precipitate (p) fractions. The total amount of protein of the supernatant fraction was 2–3 times larger than that of the precipitate fraction. Lysates (15  $\mu$ g each) and immunoprecipitates were analyzed by immunoblotting with antibodies to Cull1, FLAG, and Skp1. Asterisks show Ig heavy and light chains. To control for the fractionation, immunoblotting with an antibody to calnexin was performed. *C*, endogenous Fbs1 was immunoprecipitated with an antibody to FLAG from 100,000  $\times$  g supernatant, and precipitate fractions of differentiated PC12 cells were treated with nerve growth factor. Lysates (15  $\mu$ g each) and immunoprecipitates were analyzed by immunoblotting. The immunoblotting analysis for separated supernatant and precipitate fractions was conducted as for *B*.

between Fbs1 and its substrates does not affect the complex formation (lanes 4 and 5). The N-terminal sequence of Fbs1 called the P domain is unique and is not seen in other F-box proteins, but the removal of this domain from Fbs1 or the addition to Fbs2 did not affect the complex formation (Fbs1  $\Delta$ P and Fbs2 P1; lanes 6 and 13). Exchange of the F-box domains between Fbs1 and Fbs2 caused the loss of the Skp1 binding activity, probably due to the incorrect folding (Fbs1 F2, Fbs1  $\Delta$ PF2, Fbs2 F1, and Fbs2 PF1; lanes 7, 8, 10, and 11, respectively). However, the replacement of the Fbs1 N-terminal region (which contains P and F-box domains and linker sequence) with the Fbs2 N-terminal region rescued the complex formation (Fbs-2N1C; lane 9). In contrast, the addition of the Fbs1 N-terminal region instead of the Fbs2 N-terminal region markedly reduced the activity of Fbs2 to form the SCF complex but did not affect the Skp1 binding (Fbs-1N2C; lane 12). The linker sequences of the intervening segments between the F-box domain and the substrate-binding domain showed

lower homology than other portions between Fbs1 and Fbs2, suggesting that the Fbs1 linker sequence is responsible for impeding the SCF<sup>Fbs1</sup> complex formation. Indeed, only the Fbs1 mutant protein that contained the Fbs2 linker sequence could form the SCF complex, but the efficiency of the SCF complex formation was less than that of Fbs-2N1C (Fbs1 I2; lane 15). On the other hand, Fbs2 protein containing the Fbs1 linker sequence and the Fbs1 protein without its linker sequence did not seem to show the correct folding for Skp1 binding (Fbs2 I1 and Fbs1  $\Delta$ I; lanes 16 and 17). The Fbs1 mutant in which the F-box domain and the linker sequence are replaced with those of Fbs2 forms the SCF complex effectively. Thus, we conclude that the Fbs1 linker sequence between the F-box and substrate-binding domains hampers the SCF<sup>Fbs1</sup> complex formation.

We next compared the localization of Fbs1, Fbs2, and the mutant Fbs1 proteins capable of forming the SCF complex: Fbs-2N1C and Fbs1 I2 (Fig. 3C). Although a minor population of Fbs1 in the precipitate (p) fraction formed the SCF complex, most Fbs2 formed the SCF<sup>Fbs2</sup> complex in the supernatant (s) fraction as well as the precipitate fraction. Fbs-2N1C could form the SCF complex mainly in the supernatant fraction (Fig. 3C). Moreover, the amount of Cull1 co-immunoprecipitated with Fbs1 I2 was similar in both fractions. These results suggest that the linker sequence of Fbs1 does not only impede the formation of the SCF complex but also restricts the localization of the SCF complex bound on the ER membrane.

**Expression of Mutant Fbs1 That Forms E3 Easily Induces Proteolysis of Its Substrates**—To confirm that most Fbs1 in the cells is inactive to function as an E3 ubiquitin ligase, we next examined the ability of the mutant Fbs1 that readily forms the SCF complex (Fbs-2N1C) to ubiquitylate the substrates. It has been shown that P23H mutated rhodopsin (hereafter referred to as P23H) is an ERAD substrate, and its N-linked glycosylation is required for the degradation (15, 16). As reported previously, rhodopsin monomer is ~40–43 kDa, but the majority of P23H was detected as high molecular weight complex multimers by immunoblotting with anti-rhodopsin antibody (Fig. 4A). Wild-type Fbs1, but not the substrate-binding defective mutant Fbs1 YW, was able to associate with P23H effectively, suggesting that Fbs1 binds to P23H through its N-glycans. On the other hand,